

<sup>1</sup> Particle Kalman Filtering: A Nonlinear Bayesian  
<sup>2</sup> Framework for Ensemble Kalman Filters

<sup>3</sup> Ibrahim Hoteit<sup>1,\*</sup>, Xiaodong Luo<sup>1</sup>, and Dinh-Tuan Pham<sup>2</sup>

<sup>1</sup>King Abdullah University of Sciences and Technology, Thuwal, KSA

<sup>2</sup>Centre National de la Recherche Scientifique, Grenoble, France

Submitted to *Monthly Weather Review*

<sup>4</sup> August 2, 2011

---

\*Email: ibrahim.hoteit@kasut.edu.sa; Tel: +966-544700033

## Abstract

6 This paper investigates an approximation scheme of the optimal nonlinear  
7 Bayesian filter based on the Gaussian mixture representation of the state prob-  
8 ability distribution function. The resulting filter is similar to the particle filter,  
9 but is different from it in that, the standard weight-type correction in the par-  
10 ticle filter is complemented by the Kalman-type correction with the associated  
11 covariance matrices in the Gaussian mixture. We show that this filter is an  
12 algorithm in between the Kalman filter and the particle filter, and therefore is  
13 referred to as the particle Kalman filter (PKF).

14 In the PKF, the solution of a nonlinear filtering problem is expressed as the  
15 weighted average of an “ensemble of Kalman filters” operating in parallel. Run-  
16 ning an ensemble of Kalman filters is, however, computationally prohibitive for  
17 realistic atmospheric and oceanic data assimilation problems. For this reason,  
18 we consider the construction of the PKF through an “ensemble” of ensem-  
19 ble Kalman filters (EnKFs) instead, and call the implementation the particle  
20 EnKF (PEnKF). We show that different types of the EnKFs can be considered  
21 as special cases of the PEnKF. Similar to the situation in the particle filter,  
22 we also introduce a re-sampling step to the PEnKF in order to reduce the  
23 risk of weights collapse and improve the performance of the filter. Numerical  
24 experiments with the strongly nonlinear Lorenz-96 model are presented and  
25 discussed.

## 26 1 Introduction

27 Estimating the state of the atmosphere and the ocean has long been one of the main  
28 goals of modern science. Data assimilation, which consists of combining data and dy-  
29 namical models to determine the best possible estimate of the state of a system, is now  
30 recognized as the best approach to tackle this problem (Ghil and Malanotte-Rizzoli,  
31 1991). The strongly nonlinear character of the atmospheric and oceanic models, com-  
32 bined with their important computational burden, makes data assimilation in these  
33 systems quite challenging.

34 Based on the Bayesian estimation theory, the optimal solution of the nonlinear  
35 data assimilation problem can be obtained from the optimal nonlinear filter (ONF)  
36 (Doucet et al., 2001). This involves the estimation of the conditional probability  
37 distribution function (*pdf*) (not necessarily Gaussian) of the system state given all  
38 available measurements up to the estimation time. Knowledge of the state *pdf* allows  
39 determining different estimates of the state, such as the minimum variance estimate or  
40 the maximum a posteriori estimate (Todling, 1999). The ONF recursively operates  
41 as a succession of a correction (or analysis) step at measurement times to correct  
42 the state (predictive) *pdf* using the Bayes' rule, and a prediction step to propagate  
43 the state (analysis) *pdf* to the time of the next available observation. Although  
44 conceptually simple, the numerical implementation of the optimal nonlinear filter can  
45 be computationally prohibitive, even for systems with few dimensions (Doucet et al.,  
46 2001). Its use with atmospheric and oceanic data assimilation problems is therefore  
47 not possible because of the huge dimension of these systems.

48 In recent years, two approximation schemes of the ONF have attracted the at-  
49 tention of researchers for their potentials to tackle nonlinear and non-Gaussian data  
50 assimilation problems. One is based on the point-mass representation (mixture of  
51 Dirac functions) of the state *pdf*, and leads to the celebrated particle filter (PF)  
52 (Doucet et al., 2001; Pham, 2001; Nakano et al., 2007; Van Leeuwen, 2003, 2009).

53 The other is based on the Gaussian mixture representation of the state *pdf*, and results  
54 in a filter that is in between the Kalman filter and the particle filter (Anderson and Anderson,  
55 1999; Bengtsson et al., 2003; Chen and Liu, 2000; Hoteit et al., 2008; Luo et al., 2010;  
56 Sorenson and Alspach, 1971), as to be shown later. For this reason, we refer to this  
57 filter as the particle Kalman filter (PKF).

58 In terms of computational efficiency, the particle filter needs to generate large  
59 samples for a good approximation of the state *pdf*. In certain circumstances, in order  
60 to avoid weights collapse, the number of samples needs to scale exponentially with  
61 the dimension of the system in assimilation (Bengtsson et al., 2008), which may be  
62 infeasible for high-dimensional systems (Snyder et al., 2008). On the other hand,  
63 in some comparison studies (Han and Li, 2008; Nakano et al., 2007), it has been  
64 reported that the ensemble Kalman filter (EnKF) and its variants (Anderson, 2001;  
65 Bishop et al., 2001; Burgers et al., 1998; Evensen, 1994; Evensen and van Leeuwen,  
66 1996; Houtekamer and Mitchell, 1998; Whitaker and Hamill, 2002) can achieve lower  
67 estimation errors than the particle filter given a small ensemble size. To save space,  
68 in this paper we confine ourselves to the PKF, and make performance comparison  
69 only between the PKF and the EnKF.

70 Using a Gaussian mixture representation of the state *pdf*, the resulting PKF con-  
71 sists of an ensemble of parallel nonlinear Kalman filters (Hoteit et al., 2008; Luo et al.,  
72 2010). Different variants of the Kalman filter (KF), including the extended Kalman  
73 filter (Chen and Liu, 2000; Sorenson and Alspach, 1971), the reduced-rank Kalman  
74 filter (Hoteit et al., 2008; Luo et al., 2010), the EnKF (Anderson and Anderson, 1999;  
75 Bengtsson et al., 2003), can be used to construct the PKF. The focus of this paper  
76 is to investigate the PKF that is constructed by an ensemble of parallel EnKFs.  
77 Common to all the implementations of the PKF, the mixture of normal distributions  
78 (MON) – a more general *pdf* representation than the single Gaussian *pdf* approxi-  
79 mation in the EnKF – can be used to tackle nonlinearity and non-Gaussianity in  
80 data assimilation. On the other hand, choosing the EnKF to construct the PKF is

81 based on the consideration of computational efficiency, since the EnKF itself is a very  
82 efficient algorithm for data assimilation in high dimensional systems. In this regard,  
83 this work is very similar to the earlier works of Anderson and Anderson (1999) and  
84 Bengtsson et al. (2003), but is different from them mainly in the following aspect.

85 In Anderson and Anderson (1999) and Bengtsson et al. (2003), the PKF was con-  
86 structed without a re-sampling step. As a result, the PKF may suffer from weights  
87 collapse as in the particle filter. To overcome this problem, Bengtsson et al. (2003)  
88 considered a hybrid of the EnKF and the PKF, which, however, involves the computa-  
89 tion of the inverses of sample covariance matrices in the “global-to-local” adjustments.  
90 In doing so, it is not only computationally intensive, but also encounters singularities  
91 in computing the inverses when the ensemble size is smaller than the system dimen-  
92 sion, such that the sample covariances themselves are rank deficient. Therefore, it  
93 is not clear how the hybrid scheme in Bengtsson et al. (2003) can be applied to the  
94 scenario with the ensemble size smaller than the system dimension. For the imple-  
95 mentation of the PKF scheme in this work, we introduce a re-sampling step similar  
96 to those in Musso et al. (2001) and Stavropoulos and Titterington (2001) to tackle  
97 weights collapse. Our experience shows that, with this re-sampling step, the PKF  
98 becomes much more stable and can conduct data assimilation in the small ensemble  
99 scenario, as to be demonstrated through the numerical experiments presented in this  
100 work.

101 As may be of particular interest for the ensemble filtering community, we will show  
102 that different EnKFs can be considered as special cases of the PEnKF following our  
103 implementation. This point of view allows for a better understanding of the EnKFs’  
104 behaviors and/or their differences.

105 The paper is organized as follows. The optimal nonlinear filter is first described  
106 in section 2. The PKF and its ensemble implementation are discussed in section 3.  
107 Results of numerical experiments with the Lorenz-96 model are presented in section  
108 4. A summary of the main results and a general discussion on the potential of the

109 PEnKF for tackling realistic atmospheric and oceanic data assimilation problems  
110 concludes the paper in section 5.

## 111 2 The Optimal Nonlinear Filter

112 Starting from a random initial condition with a known probability density function,  
113 the optimal nonlinear filter provides the conditional density function of the system  
114 state given all available measurements up to the estimation time. To describe the  
115 algorithm of the optimal nonlinear filter, consider the nonlinear stochastic discrete-  
116 time dynamical system

$$\mathbf{x}_k = \mathbf{M}_k(\mathbf{x}_{k-1}) + \boldsymbol{\eta}_k, \quad (1)$$

$$\mathbf{y}_k = \mathbf{H}_k(\mathbf{x}_k) + \boldsymbol{\epsilon}_k, \quad (2)$$

117 where  $\mathbf{x}_k$  is the state vector (to be estimated), of dimension  $n$ ,  $\mathbf{y}_k$  is the observa-  
118 tion vector, of dimension  $p$ ,  $\mathbf{M}_k$  and  $\mathbf{H}_k$  are two continuously differentiable maps  
119 from  $\mathbb{R}^n$  to  $\mathbb{R}^n$  and from  $\mathbb{R}^n$  to  $\mathbb{R}^p$  respectively representing the transition and the  
120 observational operators, and  $\boldsymbol{\eta}_k$  and  $\boldsymbol{\epsilon}_k$  denote the dynamical and the observational  
121 noise, respectively. We assume that  $\boldsymbol{\eta}_k$  and  $\boldsymbol{\epsilon}_k$  are Gaussian with zero mean and non-  
122 singular covariance matrices  $\mathbf{Q}_k$  and  $\mathbf{R}_k$ , respectively, and are independent of the  
123 system state at any time instant. Under this setting, the dynamical system Eq. (1)  
124 is Markovian.

125 The optimal nonlinear filter recursively operates with a succession of prediction  
126 and correction steps as summarized below. The reader is referred to Doucet et al.  
127 (2001) for an extensive description of the filter. To simplify the notation,  $\mathbf{y}_{1:k}$  is  
128 defined as a shorthand for the set of all observations  $\mathbf{y}_1, \dots, \mathbf{y}_k$  up to and including  
129 time  $t_k$ . Let  $p_k^f(\cdot | \mathbf{y}_{1:k-1})$  be the conditional (predictive) *pdf* of  $\mathbf{x}_k$  given  $\mathbf{y}_{1:k-1}$  and  
130  $p_k^a(\cdot | \mathbf{y}_{1:k})$  be the conditional (analysis) *pdf* of  $\mathbf{x}_k$  given  $\mathbf{y}_{1:k}$ , both determined at  
131 time  $t_k$ . The filter steps are described as follows.

132     • *Prediction step*: Given the analysis  $pdf p_{k-1}^a(\cdot | \mathbf{y}_{1:k-1})$  at time  $t_{k-1}$ , the pre-  
 133     dictive  $pdf p_k^f(\cdot | \mathbf{y}_{1:k-1})$  is obtained by integrating  $p_{k-1}^a(\cdot | \mathbf{y}_{1:k-1})$  with the  
 134     model (1) to the time of the next available observation  $t_k$ . Under the assump-  
 135     tions made on the model noise  $\eta_k$ , the likelihood function for the state vector  
 136      $\mathbf{x}_{k-1}$  to transit to  $\mathbf{x}_k$  at the next time instant is described by the Gaussian  
 137      $pdf N(\mathbf{x}_k : \mathbf{M}_k(\mathbf{x}_{k-1}), \mathbf{Q}_k)$ , where  $N(\mathbf{x} : \mu, \Sigma)$  denotes the Gaussian  $pdf$  with  
 138     mean  $\mu$  and covariance  $\Sigma$ . Thus,

$$p_k^f(\mathbf{x}_k | \mathbf{y}_{1:k-1}) = \int_{\mathbb{R}^n} N(\mathbf{x}_k : \mathbf{M}_k(\mathbf{x}_{k-1}), \mathbf{Q}_k) p_{k-1}^a(\mathbf{x}_{k-1} | \mathbf{y}_{1:k-1}) d\mathbf{x}_{k-1}. \quad (3)$$

139     • *Correction step*: After a new observation  $\mathbf{y}_k$  has been made, the analysis  $pdf$   
 140      $p_k^a(\cdot | \mathbf{y}_{1:k})$  at time  $t_k$  is updated from  $p_k^f(\cdot | \mathbf{y}_{1:k-1})$  using Bayes' rule, i.e.,

$$p_k^a(\mathbf{x}_k | \mathbf{y}_{1:k}) = \frac{1}{b_k} p_k^f(\mathbf{x}_k | \mathbf{y}_{1:k-1}) N(\mathbf{y}_k : \mathbf{H}_k(\mathbf{x}_k), \mathbf{R}_k). \quad (4)$$

141     The analysis  $pdf$  is therefore obtained by multiplying the predictive  $pdf$  by the  
 142     observation likelihood function  $N(\mathbf{y}_k : \mathbf{H}_k(\mathbf{x}_k), \mathbf{R}_k)$ , and then being normalized  
 143     by  $b_k = \int_{\mathbb{R}^n} p_k^f(\mathbf{x}_k | \mathbf{y}_{1:k-1}) N(\mathbf{y}_k : H_k(\mathbf{x}_k), R_k) d\mathbf{x}_k$ .

144     While the expressions of the state  $pdf$ s can be obtained conceptually, determining  
 145     the exact values of them at each point of the state space is practically infeasible in  
 146     high dimensional systems (Doucet et al., 2001). For instance, the determination of  
 147     the predictive  $pdf$  requires the evaluation of the model  $\mathbf{M}_k(\mathbf{x})$  for a prohibitively large  
 148     number of  $\mathbf{x}$ , given that one single evaluation might already be computationally very  
 149     expensive in realistic atmospheric and oceanic applications.

150 **3 The Particle Ensemble Kalman Filter**

151 **3.1 Particle Kalman Filtering and Its Ensemble Implemen-  
152 tation**

153 Given  $N$  independent samples  $\mathbf{x}^1, \dots, \mathbf{x}^N$  from a (multivariate) density  $p$ , an esti-  
154 mator  $\hat{p}$  of  $p$  can be obtained by the kernel density estimation method (Silverman,  
155 1986), in the form of a mixture of  $N$  Gaussian *pdfs*:

$$\hat{p}(\mathbf{x}) = \frac{1}{N} \sum_{i=1}^N N(\mathbf{x} : \mathbf{x}^i, \mathbf{P}), \quad (5)$$

156 where  $\mathbf{P}$  is a positive definite matrix. Inspired from this estimator, the particle  
157 Kalman filter (PKF) approximates the conditional state *pdfs* in the optimal nonlinear  
158 filter by mixtures of  $N$  Gaussian densities of the form

$$p_k^s(\mathbf{x}_k | \mathbf{y}_{1:k}) = \sum_{i=1}^N w_k^i N(\mathbf{x}_k : \mathbf{x}_k^{s,i}, \mathbf{P}_k^{s,i}). \quad (6)$$

159 The subscript  $s$  replaces  $a$  at the analysis time and  $f$  at the prediction time. The  
160 parameters of the mixture are the weights  $w_k^i$ , the centers of the distributions  $\mathbf{x}_k^{s,i}$ ,  
161 and the covariance matrices  $\mathbf{P}_k^{s,i}$ . In particular, if  $N = 1$ ,  $p_k^s(\mathbf{x}_k | \mathbf{y}_{1:k})$  reduces to a  
162 single Gaussian *pdf*, so that the PKF reduces to the Kalman filter (KF) or its variants  
163 trivially (a non-trivial simplification will also be discussed below). Consequently, the  
164 KF and its variants can be considered special cases of the PKF.

165 Two special cases of Eq. (6) may be of particular interest. In the first case,  
166  $\mathbf{P}_k^{s,i} \rightarrow \mathbf{0}$ , such that the Gaussian *pdfs*  $N(\mathbf{x}_k : \mathbf{x}_k^{s,i}, \mathbf{P}_k^{s,i})$  tend to a set of Dirac func-  
167 tions  $\delta(\mathbf{x}_k^{s,i})$ , with the mass points at  $\mathbf{x}_k^{s,i}$ . In this case, the Gaussian mixture Eq. (6)  
168 reduces to the Monte Carlo approximation used in the particle filter (Doucet et al.,  
169 2001). In the second case, all Gaussian *pdfs*  $N(\mathbf{x}_k : \mathbf{x}_k^{s,i}, \mathbf{P}_k^{s,i})$  have (almost) identical  
170 centers and covariances, such that the Gaussian mixture Eq. (6) tends to a (sin-  
171 gle) Gaussian approximation, an assumption often used in various nonlinear Kalman  
172 filters (including the EnKF). In this sense, the PKF can be considered as a filter

173 in between the Kalman filter and the particle filter (Hoteit et al., 2008; Luo et al.,  
174 2010).

175 The main procedures of the PKF are summarized as follows. Without loss of  
176 generality, suppose that at time instant  $k - 1$ , the analysis *pdf*, after a re-sampling  
177 step, is given by  $\tilde{p}_{k-1}(\mathbf{x}_{k-1} \mid \mathbf{y}_{1:k-1}) = \sum_{i=1}^N \tilde{w}_{k-1}^i N(\mathbf{x}_{k-1} : \theta_{k-1}^i, \Phi_{k-1}^i)$ . Then by  
178 applying Eq. (3) at the prediction step, one obtains the background *pdf*, in terms of  
179 a new MON

$$p_k^f(\mathbf{x}_k \mid \mathbf{y}_{1:k-1}) \approx \sum_{i=1}^N \tilde{w}_{k-1}^i N\left(\mathbf{x}_k : \hat{\mathbf{x}}_k^{f,i}, \hat{\mathbf{P}}_k^{f,i}\right), \quad (7)$$

180 where  $\hat{\mathbf{x}}_k^{f,i}$  and  $\hat{\mathbf{P}}_k^{f,i}$  are the propagations of the mean  $\theta_{k-1}^i$  and the covariance  $\Phi_{k-1}^i$   
181 of the Gaussian component  $N(\mathbf{x}_{k-1} : \theta_{k-1}^i, \Phi_{k-1}^i)$  through the system model Eq. (1),  
182 respectively.

183 Given an incoming observation  $\mathbf{y}_k$ , one applies Eq. (4) to update  $p_k^f(\mathbf{x} \mid \mathbf{y}_{1:k-1})$   
184 to the analysis *pdf*, also in the form of an MON

$$p_k^a(\mathbf{x}_k \mid \mathbf{y}_{1:k}) = \sum_{i=1}^N w_k^i N\left(\mathbf{x}_k : \hat{\mathbf{x}}_k^{a,i}, \hat{\mathbf{P}}_k^{a,i}\right), \quad (8)$$

185 where  $\hat{\mathbf{x}}_k^{a,i}$  and  $\hat{\mathbf{P}}_k^{a,i}$  are updated from  $\hat{\mathbf{x}}_k^{f,i}$  and  $\hat{\mathbf{P}}_k^{f,i}$  through the Kalman filter or its  
186 variants, and the new weights

$$w_k^i = \frac{\tilde{w}_{k-1}^i N(\mathbf{y}_k : \mathbf{H}_k(\hat{\mathbf{x}}_k^{f,i}), \Sigma_k^i)}{\sum_{j=1}^N \tilde{w}_{k-1}^j N(\mathbf{y}_k : \mathbf{H}_k(\hat{\mathbf{x}}_k^{f,i}), \Sigma_k^j)}, \quad (9)$$

187 where  $\Sigma_k^i$  is the innovation matrix. If evaluated through the extended Kalman fil-  
188 ter,  $\Sigma_k^i = \mathbf{H}_k^i \hat{\mathbf{P}}_k^{f,i} (\mathbf{H}_k^i)^T + \mathbf{R}_k$ , with  $\mathbf{H}_k^i$  being the gradient of  $\mathbf{H}_k$  evaluated at  
189  $\hat{\mathbf{x}}_k^{f,i}$ . Alternatively, if evaluated in the context of the EnKF,  $\Sigma_k^i$  can be expressed  
190 as the covariance of the projected background ensemble onto the observation space  
191 plus the observation covariance  $\mathbf{R}_k$  (Evensen, 1994; Whitaker and Hamill, 2002). Fi-  
192 nally, a re-sampling step can be introduced to improve the performance of the PKF  
193 (Hoteit et al., 2008; Luo et al., 2010), so that the analysis *pdf* becomes  $\tilde{p}_k(\mathbf{x}_k \mid \mathbf{y}_{1:k}) =$   
194  $\sum_{i=1}^N \tilde{w}_k^i N(\mathbf{x}_k : \theta_k^i, \Phi_k^i)$ . Such a re-sampling algorithm is presented in the next section.

195        The PKF correction step can be interpreted as composed of two types of correc-  
 196        tions: a *Kalman-type correction* used to update  $\hat{\mathbf{x}}_k^{f,i}$  and  $\hat{\mathbf{P}}_k^{f,i}$  to  $\hat{\mathbf{x}}_k^{a,i}$  and  $\hat{\mathbf{P}}_k^{a,i}$ , and  
 197        a *particle-type correction* used to update the weights  $\tilde{w}_{k-1}^i$  to  $w_k^i$ . In the PKF, the  
 198        Kalman correction reduces the risk of weights collapse by allocating the estimates  
 199         $\hat{\mathbf{x}}_k^{f,i}$  (whose projections onto the observation space) far away from the observation  $\mathbf{y}_k$   
 200        relatively more weights than in the particle filter (Hoteit et al., 2008; Van Leeuwen,  
 201        2009). Indeed, Eq. (9) has the same form as in the PF (Doucet et al., 2001), but uses  
 202        the innovation matrices  $\Sigma_k^i$  to normalize the model-data misfit, rather than  $\mathbf{R}_k$ . As  
 203         $\Sigma_k^i$  are always greater than  $\mathbf{R}_k$ , the estimates that are close to the observation will  
 204        receive relatively less weights than in the PF, while those far from the observation will  
 205        receive relatively more weights. This means that the support of the local predictive  
 206        *pdf* and the observation likelihood function will be more coherent than in the PF.  
 207        Re-sampling will therefore be needed less often, so that Monte Carlo fluctuations are  
 208        reduced.

209        The main issue with the PKF is the prohibitive computational burden associated  
 210        with running an ensemble of KFs, knowing that running a Kalman filter (KF) or an  
 211        extended KF in high dimensional systems is already a challenge. To reduce compu-  
 212        tational cost, we use an ensemble of EnKFs, rather than the KF or the extended KF,  
 213        to construct the PKF. We refer to this approach as the Particle Ensemble Kalman  
 214        Filter (PEnKF). In the PEnKF, the (analysis) ensembles representing the Gaussian  
 215        components are propagated forward in time to obtain a set of background ensembles  
 216        at the next assimilation cycle. Then for each background ensemble, a stochastic or  
 217        deterministic EnKF is used to update the background ensemble to its analysis coun-  
 218        terpart. This amounts to simultaneously running a weighted ensemble of EnKFs, and  
 219        the final state estimate is the weighted average of all the EnKFs solutions.

220 **3.2 A Re-sampling Algorithm**

221 We adopt a re-sampling algorithm that combines those in Hoteit et al. (2008); Luo et al.  
 222 (2010); Pham (2001). The main idea is as follows: Given a MON, we first employ an  
 223 information-theoretic criterion used in Hoteit et al. (2008) and Pham (2001) to check  
 224 if it needs to conduct re-sampling. If there is such a need, we then re-approximate  
 225 the MON by a new MON, based on the criterion that the mean and covariance of  
 226 the new MON match those of the original MON as far as possible Luo et al. (2010).

227 More concretely, let  $p(\mathbf{x})$  be the *pdf* of the  $n$ -dimensional random vector  $\mathbf{x}$ , ex-  
 228 pressed in terms of an MON with  $N$  Gaussian *pdfs* so that

$$p(\mathbf{x}) = \sum_{i=1}^N w_i N(\mathbf{x} : \mu_i, \Sigma_i), \quad (10)$$

229 where  $w_i$  are the set of normalized weights of the Gaussian *pdfs*  $N(\mathbf{x} : \mu_i, \Sigma_i)$  with  
 230 mean  $\mu_i$  and covariance  $\Sigma_i$ , satisfying  $w_i \geq 0$  for  $i = 1, \dots, N$  and  $\sum_{i=1}^N w_i = 1$ . To  
 231 decide whether to conduct re-sampling or not, the entropy  $E_w$  of the weights  $w_i$  is  
 232 computed, which reads (Hoteit et al., 2008; Pham, 2001)

$$E_w = - \sum_{i=1}^N w_i \log w_i. \quad (11)$$

233 Ideally, when the distribution of the weights  $w_i$  is uniform, which yields the maximum  
 234 weight entropy  $E_w^u = \log N$ , there is no need to conduct re-sampling. Thus, as a  
 235 criterion, if  $E_w$  is within a certain distance  $d$  to  $E_w^u$ , i.e.,

$$E_w^u - E_w = \log N + \sum_{i=1}^N w_i \log w_i \leq d, \quad (12)$$

236 where  $d$  is a user-defined threshold, then we choose not to conduct re-sampling. In  
 237 this work we set the threshold  $d = 0.25$  following Hoteit et al. (2008).

238 In case that there is a need to conduct re-sampling, we follow the procedure  
 239 similar to that in Luo et al. (2010). Here the idea is to treat re-sampling as a *pdf*  
 240 approximation problem, in which we seek a new MON

$$\tilde{p}(\mathbf{x}) = \frac{1}{q} \sum_{i=1}^q N(\mathbf{x} : \theta_i, \Phi_i), \quad (13)$$

241 with  $q$  equally weighted Gaussian *pdfs*, to approximate the original  $p(\mathbf{x})$  in Eq. (10).  
242 In approximation, we require that the mean and covariance of  $\tilde{p}(\mathbf{x})$  be as close as  
243 possible to those of  $p(\mathbf{x})$ . To this end, we need to choose proper values of  $\theta_i$  and  $\Phi_i$   
244 in order to achieve this objective.

The means and covariances of  $p(\mathbf{x})$  and  $\tilde{p}(\mathbf{x})$ , denoted by  $\bar{\mathbf{x}}$  and  $\bar{\mathbf{P}}$ , and  $\tilde{\mathbf{x}}$  and  $\tilde{\mathbf{P}}$ , respectively, are given by

$$\bar{\mathbf{x}} = \sum_{i=1}^N w_i \mu_i, \text{ and } \bar{\mathbf{P}} = \sum_{s=1}^N w_i \left( \Sigma_i + (\mu_i - \bar{\mathbf{x}})(\mu_i - \bar{\mathbf{x}})^T \right), \quad (14a)$$

$$\tilde{\mathbf{x}} = \frac{1}{q} \sum_{i=1}^q \theta_i, \text{ and } \tilde{\mathbf{P}} = \frac{1}{q} \sum_{i=1}^q \left( \Phi_i + (\theta_i - \tilde{\mathbf{x}})(\theta_i - \tilde{\mathbf{x}})^T \right). \quad (14b)$$

245 Thus our objective is equivalent to balancing the above equation such that

$$\tilde{\mathbf{x}} = \bar{\mathbf{x}}, \text{ and } \tilde{\mathbf{P}} \approx \bar{\mathbf{P}}. \quad (15)$$

246 In the trivial case with  $q = N = 1$ , Eq. (15) can be satisfied by letting  $\theta_1 = \mu_1$  and  
247  $\Phi_1 = \Sigma_1$ , and the PEnKF reduces to an EnKF. In non-trivial cases, for simplicity  
248 in solving Eq. (15) and reducing computational cost (as to be shown later), one may  
249 choose the covariances  $\Phi_i$  to be constant, say  $\Phi_i = \Phi$ , for  $i = 1, \dots, q$ , so that

$$\frac{1}{q} \sum_{i=1}^q \theta_i = \bar{\mathbf{x}}, \text{ and } \Phi + \frac{1}{q} \sum_{i=1}^q (\theta_i - \bar{\mathbf{x}})(\theta_i - \bar{\mathbf{x}})^T \approx \bar{\mathbf{P}}. \quad (16)$$

250 When an EnKF is used to construct the PKF, one needs to represent the solution  
251 of Eq. (16) in terms of some ensembles  $\{\mathbf{X}_{en}^i, i = 1, \dots, q\}$ , where  $\mathbf{X}_{en}^i$  is a matrix  
252 containing the (analysis) ensemble of the  $i$ th Gaussian component in Eq. (13), with  
253 mean  $\theta_i$  and covariance  $\Phi$ . For simplicity, we assume that  $\mathbf{X}_{en}^i$  are all of dimension  
254  $n \times m$ , with the ensemble size  $m$  for each  $i$ . Similar results can be easily obtained in  
255 the case with non-uniform ensemble sizes.

256 We then define a constant  $c$ , called *fraction coefficient* hereafter, which satisfies  
257 that  $0 \leq c \leq 1$ . We let  $\Phi \approx c^2 \bar{\mathbf{P}}$ , so that Eq. (16) is reduced to

$$\frac{1}{q} \sum_{i=1}^q \theta_i = \bar{\mathbf{x}}, \text{ and } \frac{1}{q} \sum_{i=1}^q (\theta_i - \bar{\mathbf{x}})(\theta_i - \bar{\mathbf{x}})^T \approx (1 - c^2) \bar{\mathbf{P}}. \quad (17)$$

258 In other words, the centers  $\{\theta_i, i = 1, \dots, q\}$  can be generated as a set of state vectors  
 259 whose sample mean and covariance are  $\bar{\mathbf{x}}$  and  $(1 - c^2)\bar{\mathbf{P}}$ , respectively. After obtaining  
 260  $\theta_i$ , one can generate the corresponding ensembles  $\mathbf{X}_{en}^i$ , with the sample means and  
 261 covariances being  $\theta_i$  and  $\Phi \approx c^2\bar{\mathbf{P}}$ , respectively. How  $\theta_i$  and  $\mathbf{X}_{en}^i$  can be generated is  
 262 discussed with more details in the support material.

263 From the above discussion, we see that  $c$  is a coefficient that decides how to  
 264 divide  $\bar{\mathbf{P}}$  among  $\Phi$  and  $\frac{1}{q} \sum_{i=1}^q (\theta_i - \bar{\mathbf{x}})(\theta_i - \bar{\mathbf{x}})^T$ , so that the constraints in Eq. (16)  
 265 are satisfied. When  $c \rightarrow 0$ , we have  $\Phi \rightarrow \mathbf{0}$  so that  $\tilde{p}(\mathbf{x})$  in Eq. (13) approaches  
 266 the Monte Carlo approximation in the particle filter, with the mass points equal to  
 267  $\theta_i$ . On the other hand, when  $c \rightarrow 1$ , we have  $\frac{1}{q} \sum_{i=1}^q (\theta_i - \bar{\mathbf{x}})(\theta_i - \bar{\mathbf{x}})^T \rightarrow \mathbf{0}$ , so that  
 268 all  $\theta_i$  approach  $\bar{\mathbf{x}}$  and  $\Phi$  approaches  $\bar{\mathbf{P}}$ . As a result,  $\tilde{p}(\mathbf{x})$  in Eq. (13) approaches  
 269 the Gaussian *pdf*  $N(\mathbf{x} : \bar{\mathbf{x}}, \bar{\mathbf{P}})$ , which is essentially the assumption used in the EnKF.  
 270 In this sense, when equipped with the re-sampling algorithm, the PEnKF is a filter  
 271 in between the particle filter and the EnKF, with an adjustable parameter  $c$  that  
 272 influences its behavior.

273 We note that, when  $c \rightarrow 0$ , under the constraint of matching the first two mo-  
 274 ments, our re-sampling scheme is very close to the posterior Gaussian re-sampling  
 275 strategy used in the Gaussian particle filter (Kotecha and Djurić, 2003; Xiong et al.,  
 276 2006), in which one generates particles from a Gaussian distribution with mean and  
 277 covariance equal to those of the posterior *pdf* of the system states. As a result, there is  
 278 no guarantee that higher order moments of the new MON match those of the original  
 279 MON in our re-sampling scheme. If matching higher-order moments is a concern,  
 280 one may adopt alternative criteria, for instance, the one that aims to minimize the  
 281 distance (in certain metric) between the new MON and the original one, so that the  
 282 re-sampling procedure is recast as an optimization problem, in which one aims to  
 283 choose appropriate parameters, i.e., means and covariances of the new MON, that  
 284 satisfy the chosen criterion as far as possible. In principle, this type of parameter  
 285 estimation problem may be solved by the expectation-maximization (EM) algorithm

286 (Redner and Walker, 1984; Smith, 2007). But in practice, it is often computationally  
287 very intensive in doing so, due to the slow convergence rate of the EM algorithm  
288 and the high dimensionality of the parameter space in constructing the new MON.  
289 Therefore we do not consider this type of more sophisticated re-sampling strategy in  
290 this study.

291 For the purpose of pdf re-approximation, it is clear that the MON is not the  
292 only choice. A few alternatives are developed in the context of kernel density es-  
293 timation (KDE) (Silverman, 1986), and in principle all of them can be applied for  
294 pdf re-approximation. For instance, KDE is adopted at the re-sampling step in the  
295 regularized particle filter (RPF) (Musso et al., 2001; Stavropoulos and Titterington,  
296 2001) to construct a continuous pdf with respect the particles before re-sampling,  
297 and to draw a number of new particles from the continuous pdf afterwards. In this  
298 regard, the PEnKF is similar to the RPF, especially if the Gaussian kernel is adopted  
299 in the RPF for density estimation. However, there also exist differences. We list some  
300 of them as follows.

- 301 • The RPF first constructs a continuous pdf, and then draws a number of new  
302 particles with equal weights from the resulting pdf. In contrast, the PEnKF  
303 aims to directly approximate a MON by a new MON with equal weights.
- 304 • In the RPF, various kernels can be adopted for the purpose of constructing the  
305 continuous pdf. However, in the PEnKF, we are confined to use the MON,  
306 since we aim to build the PEnKF consisting of a set of parallel EnKFs.
- 307 • The pdf re-approximation criterion used in the PEnKF only captures the first  
308 two moments of the underlying pdf. In contrast, KDE used in the RPF in  
309 principle can yield a very good pdf estimate, provided that there are sufficient  
310 particles. In certain circumstances, though, the number of required particles  
311 may also suffer from the “curse-of-dimensionality” (Silverman, 1986, ch. 4).

### 312 3.3 Outline of the PEnKF Algorithm

313 To facilitate the comprehension of the PEnKF, here we provide an outline of the  
 314 main steps of its algorithm. To avoid distraction, we will discuss the initialization of  
 315 the PEnKF in the next section. Throughout this paper, we assume that the number  
 316  $q$  of Gaussian components at the re-sampling step and the number  $N$  of Gaussian  
 317 components at the prediction and correction steps are time invariant. This implies  
 318 the choice  $q = N$ .

319 Without loss of generality, we also assume that at time instant  $k-1$ , the posterior  
 320 pdf  $p_{k-1}^a(\mathbf{x}_{k-1} \mid \mathbf{y}_{1:k-1})$  is re-approximated, through the re-sampling step, by a mixture  
 321 model

$$\tilde{p}_{k-1}(\mathbf{x}_{k-1} \mid \mathbf{y}_{1:k-1}) = \sum_{i=1}^q \tilde{w}_{k-1}^i N(\mathbf{x}_{k-1} : \theta_{k-1,i}, \Phi_{k-1}) .$$

322 Moreover, the re-approximated analysis ensembles  $\{\mathbf{X}_{approx}^{k-1,i}, i = 1, \dots, q\}$  represent-  
 323 ing the Gaussian components  $N(\mathbf{x}_{k-1} : \theta_{k-1,i}, \Phi_{k-1})$  are also generated. The proce-  
 324 dures at the next assimilation cycle are outlined as follows.

325 • Prediction step: For  $i = 1, \dots, q$ , propagate the ensembles  $\mathbf{X}_{approx}^{k-1,i}$  forward  
 326 through Eq. (1) to obtain the corresponding background ensembles  $\mathbf{X}_{bg}^{k,i}$  at  
 327 instant  $k$ . Accordingly, the background pdf becomes

$$p_k^b(\mathbf{x}_k \mid \mathbf{y}_{1:k-1}) = \sum_{i=1}^q \tilde{w}_{k-1}^i N\left(\mathbf{x}_k : \hat{\mathbf{x}}_{k,i}^b, \hat{\mathbf{P}}_{k,i}^b\right) ,$$

328 with  $\hat{\mathbf{x}}_{k,i}^b$  and  $\hat{\mathbf{P}}_{k,i}^b$  being the sample mean and covariance of the ensemble  $\mathbf{X}_{bg}^{k,i}$ ,  
 329 respectively.

330 • Correction step: With an incoming observation  $\mathbf{y}_k$ , for each background ensem-  
 331 ble  $\mathbf{X}_{bg}^{k,i}$ ,  $i = 1, \dots, q$ , apply an EnKF to obtain the analysis mean  $\hat{\mathbf{x}}_{k,i}^a$  and the  
 332 analysis ensemble  $\mathbf{X}_{ana}^{k,i}$ . During the correction, covariance inflation and local-  
 333 ization (cf. § 4.2.2) can be conducted on the EnKF. In addition, update the  
 334 associated weights  $\tilde{w}_{k-1}^i$  to  $w_k^i$  according to Eq (9). After the corrections, the

335 analysis *pdf* becomes

$$p_k^a(\mathbf{x}_k \mid \mathbf{y}_{1:k}) = \sum_{i=1}^q w_k^i N \left( \mathbf{x}_k : \hat{\mathbf{x}}_{k,i}^a, \hat{\mathbf{P}}_{k,i}^a \right),$$

336 where  $w_k^i$  are computed according to Eq. (9) in the context of the EnKF, and

337  $\hat{\mathbf{P}}_{k,i}^a$  are the sample covariances of  $\mathbf{X}_{ana}^{k,i}$ .

338 • Re-sampling step: Use the criterion in (12) to determine whether to conduct  
339 re-sampling or not.

340 (1) If there is no need for re-sampling, then assign  $\tilde{p}_k(\mathbf{x}_k \mid \mathbf{y}_{1:k}) = p_k^a(\mathbf{x}_k \mid \mathbf{y}_{1:k})$ ,

341 and  $\mathbf{X}_{approx}^{k,i} = \mathbf{X}_{ana}^{k,i}$  for  $i = 1, \dots, q$ ;

342 (2) Otherwise,  $\tilde{p}_k(\mathbf{x}_k \mid \mathbf{y}_{1:k}) = \frac{1}{q} \sum_{i=1}^q N(\mathbf{x}_k : \theta_{k,i}, \Phi_k)$ , where parameters  $\theta_{k,i}$

343 and  $\Phi_k$  are computed following the method in § 3.2, and the associated

344 weights become  $1/q$ . The ensembles  $\mathbf{X}_{approx}^{k,i}$  are produced accordingly.

## 345 4 Numerical Experiments

### 346 4.1 Experiment Design

347 In the present work, we focus on two different implementations of the PEnKF: the first  
348 is based on the stochastic EnKF (SEnKF) of Evensen (1994) and the second based  
349 on the ensemble transform Kalman filter (ETKF) of Bishop et al. (2001). These two  
350 implementations are referred to as the PSEnKF and the PETKF, respectively.

351 The strongly nonlinear 40-dimensional system model due to Lorenz and Emanuel  
352 (1998) (LE98 model hereafter) was chosen as the testbed to evaluate and study the  
353 performance of these two filters. This model mimics the time-evolution of a scalar  
354 atmospheric quantity. It is governed by the following set of equations:

$$\frac{dx_i}{dt} = (x_{i+1} - x_{i-2}) x_{i-1} - x_i + 8, \quad i = 1, \dots, 40, \quad (18)$$

355 where the nonlinear quadratic terms simulate advection and the linear term represents  
 356 dissipation. Boundary conditions are cyclic, i.e. we define  $x_{-1} = x_{39}$ ,  $x_0 = x_{40}$ , and  
 357  $x_{41} = x_1$ . The model was numerically integrated using the Runge-Kutta fourth order  
 358 scheme from time  $t = 0$  to  $t = 35$  with a constant time step  $\Delta t = 0.05$  (which  
 359 corresponds to 6 hours in real time). To eliminate the impact of transition states, the  
 360 model trajectory between times  $t = 0$  and  $t = 25$  was discarded. The assimilation  
 361 experiments were carried out during the period  $t = 25.05$  to  $t = 35$  where the model  
 362 trajectory was considered to be the 'truth'. Reference states were then sampled  
 363 from the true trajectory and a filter performance is evaluated by how well it is able  
 364 to estimate the reference states using a perturbed model and assimilating a set of  
 365 (perturbed) observations that was extracted from the reference states.

366 In this work we consider two scenarios: one with a linear observation operator and  
 367 the other with a nonlinear operator. The concrete forms of these two observational  
 368 operators will be given in the relevant sections below.

369 The time-averaged root mean squared error (rmse for short) is used to evaluate  
 370 the performance of a filter. Given a set of  $n$ -dimensional state vectors  $\{\mathbf{x}_k : \mathbf{x}_k =$   
 371  $(x_{k,1}, \dots, x_{k,n})^T, k = 0, \dots, k_{max}\}$ , with  $k_{max}$  being the maximum time index ( $k_{max} =$   
 372 199 in our experiments), then the rmse  $\hat{e}$  is defined as

$$\hat{e} = \frac{1}{k_{max} + 1} \sum_{k=0}^{k_{max}} \sqrt{\frac{1}{n} \sum_{i=1}^n (\hat{x}_{k,i}^a - x_{k,i})^2}, \quad (19)$$

373 where  $\hat{\mathbf{x}}_k^a = (\hat{x}_{k,1}^a, \dots, \hat{x}_{k,n}^a)^T$  is the analysis state of  $\mathbf{x}_k$ .

374 A possible problem in directly using  $\hat{e}$  as the performance measure is that  $\hat{e}$  itself  
 375 may depend on some intrinsic parameters of the filters, for instance, the covariance  
 376 inflation factor and localization length scale as to be discussed later. This may lead  
 377 to inconsistent conclusions at different parameter values. To avoid this problem, we  
 378 adopted the following strategy: we relate a filter's best possible performance to the  
 379 minimum rmse  $\hat{e}_{min}$ , which is the minimum value of  $\hat{e}$  that the filter can achieve within  
 380 the chosen ranges of the filter's intrinsic parameters. In performance comparison, if

381 the minimum rmse  $\hat{e}_{min}^A$  of filter  $A$  is less than the minimum rmse  $\hat{e}_{min}^B$  of filter  $B$ ,  
 382 filter  $A$  is said to perform better than filter  $B$ .

383 **4.2 Implementation Details**

384 **4.2.1 Filter Initialization**

385 To initialize the PEnKF, we first estimate the mean and covariance of the LE98 model  
 386 over some time interval following Hoteit et al. (2008). These statistics are then used  
 387 to produce the  $pdf p_0^f(\mathbf{x}_0)$  of the background at the first assimilation cycle as a MON.

388 Concretely, the LE98 model was first integrated for a long period (between  $t = 0$   
 389 and  $t = 1000$ ) starting from an initial state that has been drawn at random. The  
 390 trajectory that falls between  $t = 50.05$  and  $t = 1000$  was used to estimate the mean  
 391  $\hat{\mathbf{x}}_{ds}$  and covariance  $\hat{\mathbf{P}}_{ds}$  of the dynamical system. To initialize  $p_0^f(\mathbf{x}_0)$  as a mixture of  
 392  $N$  Gaussian distributions

$$p_0^f(\mathbf{x}_0) = \frac{1}{N} \sum_{i=1}^N N(\mathbf{x}_0 : \mathbf{x}_0^{f,i}, \mathbf{P}_{com}), \quad (20)$$

393 where  $\mathbf{x}_0^{f,i}$  are the means, and  $\mathbf{P}_{com}$  the common covariance matrix of the Gaussian  
 394 distributions in the mixture, we draw  $N$  samples  $\mathbf{x}_0^{f,i}$  from the Gaussian distribution  
 395  $N(\mathbf{x}_0 : \hat{\mathbf{x}}_{ds}, \hat{\mathbf{P}}_{ds})$ , and set  $\mathbf{P}_{com} = \hat{\mathbf{P}}_{ds}$ . If  $\hat{\mathbf{x}}_0^f = \frac{1}{N} \sum_{i=1}^N \mathbf{x}_0^{f,i}$  denotes the sample mean of  
 396  $\mathbf{x}_0^{f,i}$ , then the covariance  $\mathbf{P}_0^f$  of  $p_0^f(\mathbf{x}_0)$  is given by

$$\mathbf{P}_0^f = \hat{\mathbf{P}}_{ds} + \frac{1}{N} \sum_{i=1}^N (\mathbf{x}_0^{f,i} - \hat{\mathbf{x}}_0^f)(\mathbf{x}_0^{f,i} - \hat{\mathbf{x}}_0^f)^T, \quad (21)$$

397 which is always larger than  $\hat{\mathbf{P}}_{ds}$ . The rationale behind this choice is not far from the  
 398 covariance inflation technique (Anderson and Anderson, 1999; Whitaker and Hamill,  
 399 2002). In practice, a data assimilation system is often subject to various errors,  
 400 such as poorly known model and observational errors, sampling errors, etc. In such  
 401 circumstances, an inflated background covariance would allocate more weights to the  
 402 incoming observation when updating the background to the analysis, making the  
 403 filter more robust (Jazwinski, 1970; Simon, 2006).

404 **4.2.2 Covariance Inflation and Localization**

405 Covariance inflation (Anderson and Anderson, 1999; Whitaker and Hamill, 2002) and  
406 localization (Hamill et al., 2001) are two popular techniques that are used to improve  
407 the stability and performance of the EnKF (Hamill et al., 2009; Van Leeuwen, 2009),  
408 especially in the small ensemble scenario. In our experiments, these two techniques  
409 are implemented for each EnKF in the PEnKF.

410 More concretely, to introduce covariance inflation to the  $i$ th EnKF at instant  $k$ ,  
411 we multiply the analysis covariance  $\hat{\mathbf{P}}_{k,i}^a$  (before the re-sampling step) by a factor  
412  $(1 + \delta)^2$ , where the scalar  $\delta \geq 0$ , called *covariance inflation factor*, is introduced as  
413 an intrinsic parameter of the EnKF. On the other hand, we follow the method in  
414 Hamill et al. (2001) to conduct covariance localization on the background covariance  
415 and its projection onto the observation space, with the tapering function (for smooth-  
416 ing out spuriously large values in covariance matrices) being the fifth order function  
417 defined in Eq. (4.10) of Gaspari and Cohn (1999). In doing so, another intrinsic  
418 scalar parameter  $l_c > 0$ , called *length scale* (Hamill et al., 2001), is introduced to  
419 the EnKF. Roughly speaking,  $l_c$  is a parameter that determines the critical distance  
420 beyond which the tapering function becomes zero.

421 **4.3 Experiments Results with a Linear Observation Opera-  
422 tor**

423 In the first scenario, we let the (synthetic) observations be generated every day (4  
424 model time steps) from the reference states using the following linear observation  
425 system

$$\mathbf{y}_k = (x_{k,1}, x_{k,3}, \dots, x_{k,39})^T + \mathbf{v}_k, \quad (22)$$

426 where only the odd state variables  $x_{k,i}$  ( $i = 1, 3, \dots, 39$ ) of the system state  $\mathbf{x}_k \equiv$   
427  $(x_{k,1}, \dots, x_{k,40})^T$  at time index  $k$  are observed. The observation noise  $\mathbf{v}_k$  follows the  
428 20-dimensional Gaussian distribution  $N(\mathbf{v}_k : \mathbf{0}, \mathbf{I}_{20})$  with  $\mathbf{I}_{20}$  being the  $20 \times 20$  identity

429 matrix.

#### 430 4.3.1 Effect of the Number of Gaussian Distributions

431 In the first experiment we examine the effect of the number of Gaussian distributions  
432 on the performance of the PSEnKF and the PETKF. The experiment settings are as  
433 follows.

434 We initialize the pdf  $p_0^f(\mathbf{x}_0)$  with  $N$  Gaussian *pdfs*. In our experiments we let  $N$   
435 take values between 1 and 60. Since it is costly to carry out the computation for  
436 each integer in this interval, we choose to let  $N$  increase from 1 to 10, with an even  
437 increment of 1 each time, and then increase it from 15 to 60, with a larger incre-  
438 ment of 5 each time, as  $N$  becomes larger. For convenience, we denote this choice  
439 by  $N \in \{1 : 1 : 10, 15 : 5 : 60\}$ , where the notation  $v_{min} : v_{inc} : v_{max}$  represents a  
440 set of values increasing from  $v_{min}$  to  $v_{max}$ , with an even increment of  $v_{inc}$  each time.

441 If there is a need to conduct re-sampling, we re-approximate the analysis MON by  
442 a new MON with equal weights and with the same number of normal distributions.

443 In doing so, we introduce a new parameter, i.e., the fraction coefficient  $c$  defined in  
444 § 3.2, to the PSEnKF/PETKF. To examine its effect on the performance of the  
445 filter, we let  $c \in \{0.05 : 0.1 : 0.95\}$ . The ensemble size is set to  $m = 20$  in each  
446 SEnKF/ETKF, which is relatively small compared to the system dimension 40. In  
447 this case, it is customary to conduct covariance inflation (Anderson and Anderson,  
448 1999; Whitaker and Hamill, 2002) and localization (Hamill et al., 2001) to improve  
449 the robustness and performance of the filters (Hamill et al., 2009; Van Leeuwen,  
450 2009). The impacts of covariance inflation and localization on the performance of the

451 EnKF have been examined in many works, see, for example, Whitaker and Hamill  
452 (2002). In our experiments we let the covariance inflation factor  $\delta = 0.02$ . We follow  
453 the settings in Luo et al. (2010, § 7.2.3) to conduct covariance localization and choose  
454 the length scale  $l_c = 50$ . To reduce statistical fluctuations, we repeat the experiments  
455 for 20 times, each time with a randomly drawn initial background ensemble, but the

456 same true trajectory and the corresponding observations. The same repetition setting  
457 is adopted in all the other experiments.

458 In Fig. 1 we show the rms errors of both the PSEnKF and PETKF as functions  
459 of the fraction coefficient  $c$  and the number  $N$  of Gaussian *pdfs*. First, we examine  
460 how the rmse of the PSEnKF changes with  $c$  when  $N$  is fixed. In Fig. 1(a), if  $N$   
461 is relatively small (say  $N < 40$ ), the rmse tends to decrease as  $c$  increases. For  
462 larger  $N$  (say  $N = 55$ ), the rmse of the filter exhibits the bell-shape behavior: at  
463 the beginning it increases when  $c$  grows from 0; after  $c$  becomes relatively large  
464 (say  $c = 0.4$ ), further increasing  $c$  reduces the rmse instead. Next, we examine the  
465 behavior of the rmse of the PSEnKF with respect to  $N$  when  $c$  is fixed. When  $c$  is  
466 relatively small (say  $c = 0.1$ ), the rmse exhibits the U-turn behavior: at the beginning  
467 it intends to decrease as  $N$  grows; after  $N$  becomes relatively large (say  $N = 45$ ),  
468 further increasing  $N$  increases the rmse instead. When  $c$  is larger, say,  $c = 0.6$ , the  
469 rmse appears less sensitive to the change of  $N$ . However, for even larger values of  $c$ ,  
470 say,  $c = 0.9$ , the rmse appears to monotonically decrease with  $N$ .

471 The behavior of the PETKF (cf. Fig. 1(b)) with respect to the changes of  $N$  and  
472  $c$  is similar to that of the PSEnKF. Therefore we do not repeat its description here.

473 To examine the minimum rms errors  $\hat{e}_{min}$  of the PSEnKF and the PETKF within  
474 the tested values of  $c$  and  $N$ , we plot  $\hat{e}_{min}$  of both filters as functions of  $N$  in Fig. 2.  
475 The  $\hat{e}_{min}$  of both filters tends to decrease as the number  $N$  of Gaussian distributions  
476 increases, though there also exhibit certain local minima. The PSEnKF achieves its  
477 lowest  $\hat{e}_{min}$  at  $N = 60$ , while the PETKF at  $N = 50$ . As  $N$  grows, both the PSEnKF  
478 and the PETKF tend to have lower  $\hat{e}_{min}$  than their corresponding base filters, the  
479 SEnKF and the ETKF (corresponding to the PSEnKF and the PETKF with  $N = 1$ ,  
480 as discussed in § 3.2), respectively. This confirms the benefit of accuracy improvement  
481 by using the PEnKF instead of an EnKF. A comparison between the PSEnKF and  
482 the PETKF shows that the PETKF performs better than the PSEnKF when the  
483 number  $N$  of Gaussian distributions is relatively small (say,  $N \leq 7$ ). However, as

484  $N$  becomes larger, the PSEnKF outperforms its ETKF-based counterpart instead.  
485 Similar phenomena can also be observed in other experiments, as to be shown later.

486 **4.3.2 Effect of the Ensemble Size**

487 In the second experiment we examine the effect of the ensemble size of each SEnKF/ETKF  
488 in the PEnKF, on the performance of the PSEnKF/PETKF. For reference, we also  
489 examine the performance of the SEnKF and the ETKF under various ensemble sizes.  
490 The experiment settings are as follows. For the PSEnKF and the PETKF, we let the  
491 ensemble size  $m$  of each EnKF take values from the set  $\{20, 40, 80, 100, 200, 400, 800, 1000\}$ .  
492 For a single SEnKF/ETKF, we let  $m \in \{20, 40, 60, 80, 100, 200, 400, 600, 800, 1000\}$ ,  
493 with two more values at 60 and 600.

494 In the PSEnKF and the PETKF, we also vary the fraction coefficient  $c$  such that  
495  $c \in \{0.05 : 0.1 : 0.95\}$ . We fix the number  $N$  of Gaussian *pdfs*, i.e., the number of  
496 ensemble filters, to be 3. To conduct covariance inflation, we let the inflation factor  
497  $\delta = 0.02$ . We choose to conduct covariance localization, and set the length scale  
498  $l_c = 50$ , only if the ensemble size  $m$  is not larger than the dimension 40 of the LE98  
499 model. No covariance localization was conducted if  $m > 40$ . Our experience shows  
500 that, for  $m > 40$ , the benefit of conducting localization is not significant even if the  
501 length scale  $l_c$  is properly chosen, while an improper value of  $l_c$  is more likely to  
502 deteriorate the filter performance. To reduce statistical fluctuations, the experiments  
503 are again repeated for 20 times.

504 In Fig. 3 we show the rms errors of the SEnKF and the ETKF as functions of  
505 the ensemble size  $m$ . The rmse of the ETKF exhibits a U-turn behavior. The rmse  
506 of the ETKF monotonically decreases as long as  $m < 100$ . Beyond that, the rmse  
507 monotonically increases instead as  $m$  increases. On the other hand, the SEnKF  
508 exhibits a different behavior. Its rmse decreases for  $m \leq 200$ , and then reaches a  
509 plateau where the rmse remains almost unchanged as  $m$  further increases.

510 Fig. 4 plots the rms errors of the PSEnKF and the PETKF as functions of the

fraction coefficient  $c$ , and the ensemble size  $m$  in the SEnKF and the ETKF used to construct the corresponding PEnKFs. The rms errors, as functions of the ensemble size  $m$  (with fixed  $c$ ), are consistent with our observations in Fig. 3. On the other hand, for both PEnKFs, their rms errors tend to decrease as the fraction coefficient  $c$  increases.

Per analogy to the first experiment, Fig. 5 plots the minimum rms errors  $\hat{e}_{min}$  of the PSEnKF and the PETKF within the tested fraction coefficient  $c$  and the ensemble size  $m$ . A comparison between Figs. 5 and 3 shows that, the minimum rms errors  $\hat{e}_{min}$  of the PEnKFs behave very similarly to the rms errors of their corresponding EnKFs in Fig. 3. Moreover, the values of  $\hat{e}_{min}$  in Fig. 5 tends to be lower than the corresponding rms errors in Fig. 3, indicating the benefit of accuracy improvement in using the PEnKFs. Again, a comparison between the PSEnKF and the PETKF shows that the PETKF performs better than the PSEnKF when the ensemble size  $m$  is relatively small (say,  $m \leq 40$ ). However, as  $m$  becomes larger, the PSEnKF outperforms the PETKF instead.

#### 4.4 Experiments Results with a Nonlinear Observation Operator

In the second scenario, we introduce nonlinearity to the observation system. To this end, we let the observations be generated by the following nonlinear process

$$\mathbf{y}_k = 0.05(x_{k,1}^2, \dots, x_{k,39}^2)^T + \mathbf{v}_k \quad (23)$$

for every 4 model time steps. In Eq. (23), again only the odd state variables  $x_{k,i}$  ( $i = 1, 3, \dots, 39$ ) of the system state  $\mathbf{x}_k \equiv (x_{k,1}, \dots, x_{k,40})^T$  at time index  $k$  are observed. The observation noise  $\mathbf{v}_k$  also follows the 20-dimensional Gaussian distribution  $N(\mathbf{v}_k : \mathbf{0}, \mathbf{I}_{20})$ . We conduct the same experiments as those in the case of linear observation operator.

535 **4.4.1 Effect of the Number of Gaussian Distributions**

536 We first examine the effect of the number of Gaussian distributions. The experiment  
537 settings are the same as those in § 4.3.1. Concretely, For either the PSEnKF or the  
538 PETKF, the number of Gaussian distributions  $N \in \{1 : 1 : 10, 15 : 5 : 60\}$ , the  
539 fraction coefficient  $c \in \{0.05 : 0.1 : 0.95\}$ . For each individual SEnKF/ETKF in  
540 the PEnKF, the ensemble size  $m = 20$ , the covariance inflation factor  $\delta = 0.02$  and  
541 the length scale  $l_c = 50$  for covariance localization. As before, the experiments are  
542 repeated for 20 times to reduce statistical fluctuations.

543 Fig. 6 plots the rms errors of both the PSEnKF and the PETKF as functions of  
544 the fraction coefficient  $c$  and the number  $N$  of Gaussian *pdfs*. When  $c$  and  $N$  changes,  
545 both the PSEnKF and the PETKF behave very similar to their counterparts in the  
546 linear case. The rms errors of the filters tend to decrease as  $N$  increases, meaning  
547 that the PSEnKF/PETKF with  $N > 1$  in general performs better than the stochastic  
548 EnKF /ETKF (corresponding to the case  $N = 1$  in the PEnKF), consistent with the  
549 results obtained in the linear observer case.

550 We also examine the minimum rms errors  $\hat{e}_{min}$  of the PSEnKF and the PETKF  
551 within the tested values of  $c$  and  $N$ . Fig. 7 plots  $\hat{e}_{min}$  as functions of  $N$ . For the  
552 PSEnKF, the lowest  $\hat{e}_{min}$  is achieved at  $N = 50$ . And for the PETKF, its  $\hat{e}_{min}$  tends  
553 to decrease within the tested range of  $N$ , and achieves its minimum at  $N = 60$ . The  
554 PEnKF with more than one Gaussian distributions ( $N > 1$ ) performs better than  
555 the corresponding EnKF ( $N = 1$ ). In addition, a comparison between the PSEnKF  
556 and the PETKF shows again that the PETKF performs better than the PSEnKF  
557 when the number  $N$  of Gaussian distributions is relatively small, but tends to become  
558 worse as  $N$  increases.

559 A comparison between Figs. 2 and 7 shows that the rmse of a filter (e.g. the  
560 PSEnKF at  $N = 2$ ) with a nonlinear observer sometimes may be lower than that  
561 of the same filter with a linear observer<sup>1</sup>. This seemingly counter-intuitive result

---

<sup>1</sup>The result of comparison would also depend on the filter in use, its configuration, the system in

happens possibly because in such situations, the effect of sampling error due to the relatively small ensemble size dominates the effect of nonlinearity in the observation system. However, as the number  $N$  of Gaussian distributions increases, the effect of nonlinearity becomes more prominent so that the rmse with a nonlinear observer tends to be higher than that with a linear one. Similar phenomenon can also be found by comparing Figs. 3 and 5 with Figs. 8 and 10 (to be shown below), respectively, at different ensemble sizes.

#### 4.4.2 Effect of the Ensemble Size

In the second experiment we examine the effect of the ensemble size in each ensemble filter on the performance of the corresponding PEnKF. For reference, we also examine the performance of the SEnKF and the ETKF under various ensemble sizes. The experiment settings are the same as those in § 4.3.2. In the PSEnKF and PETKF, we choose the fraction coefficient  $c \in \{0.05 : 0.1 : 0.95\}$ . We also choose the number of ensemble filters in each PEnKF to be 3. For each individual EnKF in the corresponding PEnKF, we let the ensemble size  $m$  take values from the set  $\{20, 40, 80, 100, 200, 400, 800, 1000\}$ , and for the experiments on the single EnKF, we let  $m \in \{20, 40, 60, 80, 100, 200, 400, 600, 800, 1000\}$ . To conduct covariance inflation and localization in each individual EnKF, we choose the inflation factor  $\delta = 0.02$ , and the length scale  $l_c = 50$ . As in § 4.3.2, covariance localization is conducted only if the ensemble size  $m$  is no larger than the dimension 40.

Fig. 8 shows the rms errors of the SEnKF and the ETKF as functions of the ensemble size  $m$ . For both filters, their rms errors decrease as the ensemble size  $m$  increases. The ETKF performs better than the SEnKF in the small sample scenario with  $m = 20$ . But as  $m$  increases, the SEnKF outperforms the ETKF instead. In particular, divergence in the ETKF occurs if  $m > 400$ , which did not happen in the linear observer case (cf. Fig. 3). On the other hand, the rmse of the SEnKF appears

---

assimilation, and so on, and therefore may change from case to case.

588 to reach a plateau for  $m > 400$ , similar to the linear observer case. Comparing Fig. 8  
589 with Fig. 3, it is easy to see that, except for the stochastic EnKF at  $m = 20$ , the  
590 presence of nonlinearity in the observer deteriorates the performance of the ensemble  
591 filters.

592 Fig. 9 plots the rms errors of the PSEnKF and the PETKF as functions of the  
593 fraction coefficient  $c$ , and the ensemble size  $m$  in the corresponding SEnKF and the  
594 ETKF, respectively. In the PSEnKF (cf. Fig. 9(a)), the rmse tends to decrease as  
595 both  $c$  and  $m$  increases when the ensemble size  $m \leq 800$ . However, when  $m > 800$ , the  
596 impact of  $m$  on the filter performance is not significant, which is consistent with the  
597 results in Fig. 8. On the other hand, in the PETKF (cf. Fig. 9(b)), filter divergence  
598 occurs for  $m > 200$ , which is why we only report its rmse with  $m \leq 200$  in Fig. 9(b),  
599 where the rmse of the PETKF appears to be a monotonically decreasing function of  
600  $m$  and  $c$ .

601 In analogy to the first experiment, Fig. 10 plots the minimum rms errors  $\hat{e}_{min}$  of  
602 the PSEnKF and the PETKF within the tested fraction coefficient  $c$  and ensemble  
603 size  $m$ . One may observe that, similar to the SEnKF and the ETKF themselves, the  
604  $\hat{e}_{min}$  of both the PSEnKF and the PETKF decrease as  $m$  increases. However, for the  
605 PETKF, divergence occurs if  $m > 200$ , rather than  $m > 400$  as in Fig. 8, but overall  
606 its rmse is closer to that obtained in the PSEnKF. Meanwhile, a comparison between  
607 Fig. 8 and Fig. 10 shows that the PEnKFs perform better than the corresponding  
608 EnKFs. Also, a comparison between Fig. 5 and 10 shows that, except for the PSEnKF  
609 at  $m = 20$ , the nonlinearity in the observer again deteriorates the performance of the  
610 ensemble filters.

## 611 5 Discussion

612 This paper presented a discrete solution of the optimal nonlinear filter, called the par-  
613 ticle Kalman filter (PKF), based on the Gaussian mixture representation of the state

614 *pdf* given the observations. The PKF solves the nonlinear Bayesian correction step by  
615 complementing the Kalman filter-like correction step of the particles with a particle  
616 filter-like correction step of the weights. The PKF simultaneously runs a weighted  
617 ensemble of the Kalman filters in parallel. This is far beyond our computing capabil-  
618 ities when dealing with computationally demanding systems, as the atmospheric and  
619 oceanic models. Therefore, to reduce computational cost, one may instead consider  
620 a low-rank parametrization of the Gaussian mixture covariance matrices of the state  
621 *pdfs*. An efficient way to do that is to resort to the ensemble Kalman filter (EnKF)  
622 and use an EnKF-like method to update each component of the Gaussian mixture  
623 *pdfs*. This amounts to running a weighted ensemble of the EnKFs. In this work, the  
624 PKF was implemented using the stochastic EnKF and a deterministic EnKF, the  
625 ensemble transform Kalman filter (ETKF). We call this type of implementation the  
626 particle ensemble Kalman filter (PEnKF).

627 The PEnKF sets a nonlinear Bayesian filtering framework that encompasses the  
628 EnKF methods as a special case. As in the EnKF, the Kalman correction in the  
629 PEnKF attenuates the degeneracy of the ensemble by allocating the ensemble mem-  
630 bers far away from the incoming observation relatively more weights than in the  
631 particle filter, so that the filter can operate with reasonable size ensembles. To fur-  
632 ther improve the performance of the PEnKF, we also introduced to the PEnKF a  
633 re-sampling step similar to that used in the regularized particle filter (Musso et al.,  
634 2001; Stavropoulos and Titterington, 2001).

635 The stochastic EnKF and ETKF-based PEnKFs, called the PSEnKF and the  
636 PETKF, respectively, were implemented and their performance was investigated with  
637 the strongly nonlinear Lorenz-96 model. These filters were tested with both linear  
638 and nonlinear observation operators. Experiments results suggest that the PSEnKF  
639 and the PETKF outperform their corresponding EnKFs. It was also found that the  
640 ETKF outperforms the stochastic EnKF for small size ensembles while the stochas-  
641 tic EnKF exhibits better performance for large size ensembles. We argued that this

happens because the EnKF endures less observational sampling errors when the ensemble size is large. Another reason would also be the better approximation of the PEnKF distributions provided by the stochastic EnKF compared to the ETKF. This was also true for their PEnKF counterparts. Overall, the conclusions from the numerical results obtained with the linear and nonlinear observation operators were not fundamentally different, except that in general better estimation accuracy was achieved with the linear observer when the sampling error is not the dominant factor. The results also suggest that the PEnKFs could more benefit from the use of more components in the mixture of normals (MON) and larger ensembles in the EnKFs in the nonlinear observations case.

Future work will focus on developing and testing new variants of the PEnKF that applies more efficient approximations, in term of computational cost, to update the mixture covariance matrices. Another direction for improvement would be also to work on localizing the correction step of the particle weights (Van Leeuwen, 2009). Our final goal is to develop a set of computationally feasible suboptimal PEnKFs that can outperform the EnKF methods at reasonable computational cost. As stated by Anderson (2003), developing filters in the context of the optimal nonlinear filtering problem, rather than starting from the Kalman filter, should lead to a more straightforward understanding of their capabilities.

The paper further discussed how the PEnKF can also be used as a general framework to simultaneously run several assimilation systems. We believe that this approach provides a framework to merge the solutions of different EnKFs, or to develop hybrid EnKF-variational methods. Work in this direction is under investigation.

## Acknowledge

We would like to thank the three anonymous reviewers for their valuable comments and suggestions. Ibrahim Hoteit was partially supported by ONR grant N00014-08-

668 1-0554.

669 **References**

670 Anderson, J., 2003: A local least squares framework for ensemble filtering. *Mon. Wea.  
671 Rev.*, **131** (4), 634–642.

672 Anderson, J. L., 2001: An ensemble adjustment Kalman filter for data assimilation.  
673 *Mon. Wea. Rev.*, **129**, 2884–2903.

674 Anderson, J. L. and S. L. Anderson, 1999: A Monte Carlo implementation of the  
675 nonlinear filtering problem to produce ensemble assimilations and forecasts. *Mon.  
676 Wea. Rev.*, **127**, 2741–2758.

677 Bengtsson, T., P. Bickel, and B. Li, 2008: Curse-of-dimensionality revisited: Collapse  
678 of the particle filter in very large scale systems. *IMS Collections*, **2**, 316–334.

679 Bengtsson, T., C. Snyder, and D. Nychka, 2003: Toward a nonlinear ensemble filter  
680 for high-dimensional systems. *J. Geophys. Res.*, **108**, 8775.

681 Bishop, C. H., B. J. Etherton, and S. J. Majumdar, 2001: Adaptive sampling with  
682 ensemble transform Kalman filter. Part I: theoretical aspects. *Mon. Wea. Rev.*,  
683 **129**, 420–436.

684 Burgers, G., P. J. van Leeuwen, and G. Evensen, 1998: On the analysis scheme in  
685 the ensemble Kalman filter. *Mon. Wea. Rev.*, **126**, 1719–1724.

686 Chen, R. and J. Liu, 2000: Mixture Kalman filters. *Journal of the Royal Statistical  
687 Society: Series B (Statistical Methodology)*, **62** (3), 493–508.

688 Doucet, A., N. De Freitas, and N. Gordon, (Eds.) , 2001: *Sequential Monte Carlo  
689 methods in practice*. Springer Verlag.

690 Evensen, G., 1994: Sequential data assimilation with a nonlinear quasi-geostrophic  
691 model using Monte Carlo methods to forecast error statistics. *J. Geophys. Res.*,  
692 **99(C5)**, 10 143–10 162.

693 Evensen, G. and P. J. van Leeuwen, 1996: Assimilation of geosat altimeter data  
694 for the aghulas current using the ensemble Kalman filter with a quasi-geostrophic  
695 model. *Mon. Wea. Rev.*, **124**, 85–96.

696 Gaspari, G. and S. E. Cohn, 1999: Construction of correlation functions in two and  
697 three dimensions. *Quart. J. Roy. Meteor. Soc.*, **125**, 723 – 757.

698 Ghil, M. and P. Malanotte-Rizzoli, 1991: Data assimilation in meteorology and  
699 oceanography. *Adv. Geophys.*, **33**, 141–266.

700 Hamill, T. M., J. S. Whitaker, J. L. Anderson, and C. Snyder, 2009: Comments  
701 on “Sigma-point Kalman filter data assimilation methods for strongly nonlinear  
702 systems”. *Journal of the Atmospheric Sciences*, **66**, 3498–3500.

703 Hamill, T. M., J. S. Whitaker, and C. Snyder, 2001: Distance-dependent filtering of  
704 background error covariance estimates in an ensemble Kalman filter. *Mon. Wea.  
705 Rev.*, **129**, 2776–2790.

706 Han, X. and X. Li, 2008: An evaluation of the nonlinear/non-Gaussian filters for the  
707 sequential data assimilation. *Remote Sensing of Environment*, **112**, 1434 – 1449.

708 Hoteit, I., D. T. Pham, and J. Blum, 2002: A simplified reduced order Kalman  
709 filtering and application to altimetric data assimilation in Tropical Pacific. *Journal  
710 of Marine Systems*, **36**, 101–127.

711 Hoteit, I., D. T. Pham, G. Triantafyllou, and G. Korres, 2008: A new approximate  
712 solution of the optimal nonlinear filter for data assimilation in meteorology and  
713 oceanography. *Mon. Wea. Rev.*, **136**, 317–334.

714 Houtekamer, P. L. and H. L. Mitchell, 1998: Data assimilation using an ensemble  
715 Kalman filter technique. *Mon. Wea. Rev.*, **126**, 796–811.

716 Jazwinski, A. H., 1970: *Stochastic Processes and Filtering Theory*. Academic Press.

717 Kotecha, J. and P. Djurić, 2003: Gaussian particle filtering. *Signal Processing, IEEE  
718 Transactions on*, **51** (10), 2592–2601.

719 Lorenz, E. N. and K. A. Emanuel, 1998: Optimal sites for supplementary weather  
720 observations: Simulation with a small model. *J. Atmos. Sci.*, **55**, 399–414.

721 Luo, X., I. M. Moroz, and I. Hoteit, 2010: Scaled unscented transform Gaussian sum  
722 filter: Theory and application. *Physica D*, **239**, 684–701.

723 Musso, C., N. Oudjane, and F. L. Gland, 2001: Improving regularized particle fil-  
724 ters. *Sequential Monte Carlo methods in practice*, A. Doucet, N. de Freitas, and  
725 N. Gordon, Eds., Springer-Verlag, chap. 12, 247–271.

726 Nakano, S., U. G., and T. Higuchi, 2007: Merging particle filter for sequential data  
727 assimilation. *Nonlin. Processes Geophys.*, **14**, 395–408.

728 Pham, D. T., 2001: Stochastic methods for sequential data assimilation in strongly  
729 nonlinear systems. *Mon. Wea. Rev.*, **129**, 1194–1207.

730 Redner, R. and H. Walker, 1984: Mixture densities, maximum likelihood and the em  
731 algorithm. *SIAM review*, **26** (2), 195–239.

732 Silverman, B. W., 1986: *Density Estimation for Statistics and Data Analysis*. Chap-  
733 man & Hall.

734 Simon, D., 2006: *Optimal State Estimation: Kalman, H-Infinity, and Nonlinear  
735 Approaches*. Wiley-Interscience, 552 pp.

736 Smith, K. W., 2007: Cluster ensemble Kalman filter. *Tellus*, **59A**, 749–757.

737 Snyder, C., T. Bengtsson, P. Bickel, and J. Anderson, 2008: Obstacles to high-  
738 dimensional particle filtering. *Mon. Wea. Rev.*, **136**, 4629–4640.

739 Sorenson, H. W. and D. L. Alspach, 1971: Recursive Bayesian estimation using  
740 Gaussian sums. *Automatica*, **7**, 465 – 479.

741 Stavropoulos, P. and D. M. Titterington, 2001: Improved particle filters and smooth-  
742 ing. *Sequential Monte Carlo methods in practice*, A. Doucet, N. de Freitas, and  
743 N. Gordo, Eds., Springer-Verlag, chap. 14, 295–317.

744 Todling, R., 1999: Estimation theory and foundations of atmospheric data assimila-  
745 tion. 187 pp., DAO Office Note.

746 Van Leeuwen, P. J., 2003: A variance minimizing filter for large-scale applications.  
747 *Mon. Wea. Rev.*, **131**, 2071–2084.

748 Van Leeuwen, P. J., 2009: Particle filtering in geophysical systems. *Mon. Wea. Rev.*,  
749 **137**, 4089–4114.

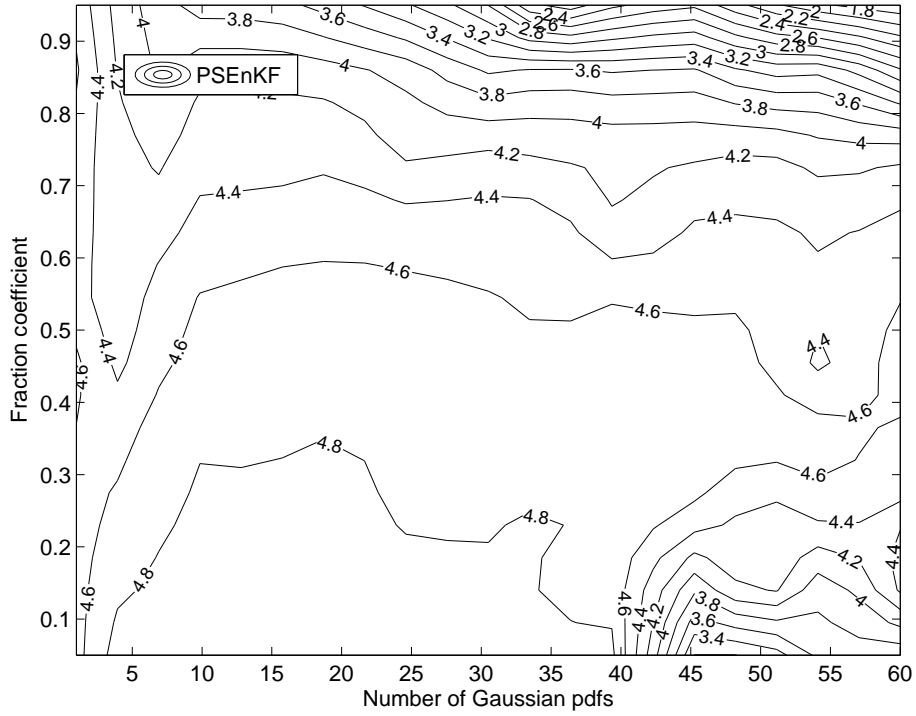
750 Whitaker, J. S. and T. M. Hamill, 2002: Ensemble data assimilation without per-  
751 turbed observations. *Mon. Wea. Rev.*, **130**, 1913–1924.

752 Xiong, X., I. Navon, and B. Uzunoglu, 2006: A note on the particle filter with  
753 posterior Gaussian resampling. *Tellus A*, **58** (4), 456–460.

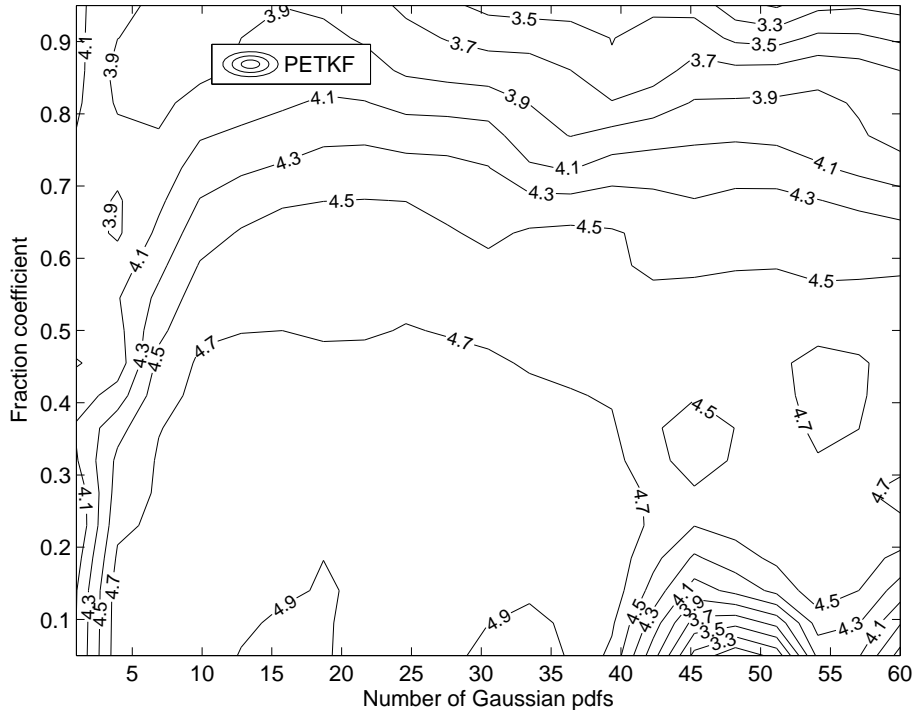
754 **List of Figures**

755 1	RMS errors (over 20 experiments) of the stochastic EnKF- and ETKF- 756 based PEnKFs (with a fixed ensemble size of 20 in each ensemble filter) 757 as the functions of the fraction coefficient and the number of Gaussian 758 <i>it</i> pdfs in the MON. . . . .	33
759 2	Minimum rms errors $\hat{e}_{min}$ (over 20 experiments) of the stochastic EnKF- 760 and ETKF-based PEnKFs (with a fixed ensemble size of 20 in each 761 ensemble filter) as the function of the number of Gaussian <i>pdfs</i> in the 762 MON. . . . .	34
763 3	RMS errors (over 20 experiments) of the stochastic EnKF and the 764 ETKF as the functions of the ensemble size. . . . .	35
765 4	RMS errors (over 20 experiments) of the stochastic EnKF- and ETKF- 766 based PEnKFs (with a fixed number of Gaussian <i>pdfs</i> of 3 in each PKF) 767 as the functions of the fraction coefficient and the ensemble size of the 768 ensemble filter. . . . .	36
769 5	Minimum rms errors $\hat{e}_{min}$ (over 20 experiments) of the stochastic EnKF- 770 and ETKF-based PEnKFs (with a fixed number of Gaussian <i>pdfs</i> of 771 3 in each PKF) as the function of the ensemble size in each ensemble 772 filter. . . . .	37
773 6	RMS errors (over 20 experiments) of the stochastic EnKF- and ETKF- 774 based PEnKFs (with a fixed ensemble size of 20 in each ensemble filter) 775 as the functions of the fraction coefficient and the number of Gaussian 776 <i>pdfs</i> in the MON. . . . .	38
777 7	Minimum rms errors $\hat{e}_{min}$ (over 20 experiments) of the stochastic EnKF- 778 and ETKF-based PEnKFs (with a fixed ensemble size of 20 in each 779 ensemble filter) as the function of the number of Gaussian <i>pdfs</i> in the 780 MON. . . . .	39

781	8	RMS errors (over 20 experiments) of the stochastic EnKF and the				
782		ETKF as the functions of the ensemble size. . . . .	40			
783	9	RMS errors (over 20 experiments) of the stochastic EnKF- and ETKF-				
784		based PEnKFs (with a fixed number of Gaussian <i>pdf</i> s of 3 in each PKF)				
785		as the functions of the fraction coefficient and the ensemble size of the				
786		ensemble filter. In Fig. 9(b) the ensemble size in each ensemble filter				
787		is only up to 200. Divergence occurs in the ETKF-based PKF with				
788		ensemble sizes in each ensemble filter larger than 200. . . . .	41			
789	10	Minimum rms errors $\hat{e}_{min}$ (over 20 experiments) of the stochastic EnKF-				
790		and ETKF-based PEnKFs (with a fixed number of Gaussian <i>pdf</i> s of				
791		3 in each PKF) as the function of the ensemble size in each ensemble				
792		filter. . . . .	42			



(a) Stochastic EnKF-based PKF



(b) ETKF-based PKF

Figure 1: RMS errors (over 20 experiments) of the stochastic EnKF- and ETKF-based PEnKFs (with a fixed ensemble size of 20 in each ensemble filter) as the functions of the fraction coefficient and the number of Gaussian it pdfs in the MON.  
 33

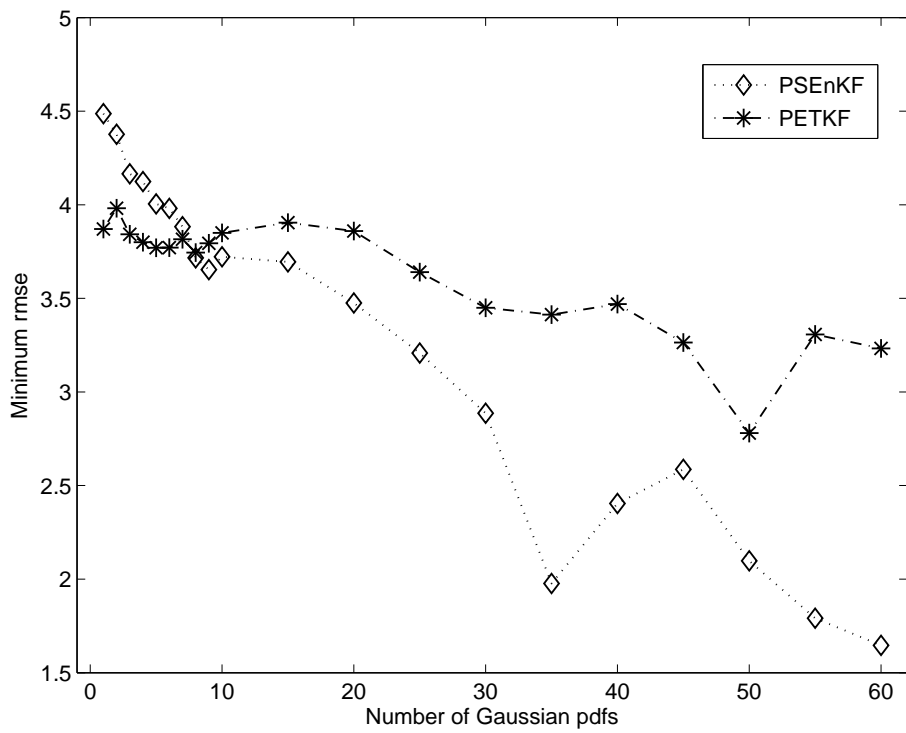


Figure 2: Minimum rms errors  $\hat{e}_{min}$  (over 20 experiments) of the stochastic EnKF- and ETKF-based PEnKFs (with a fixed ensemble size of 20 in each ensemble filter) as the function of the number of Gaussian *pdfs* in the MON.

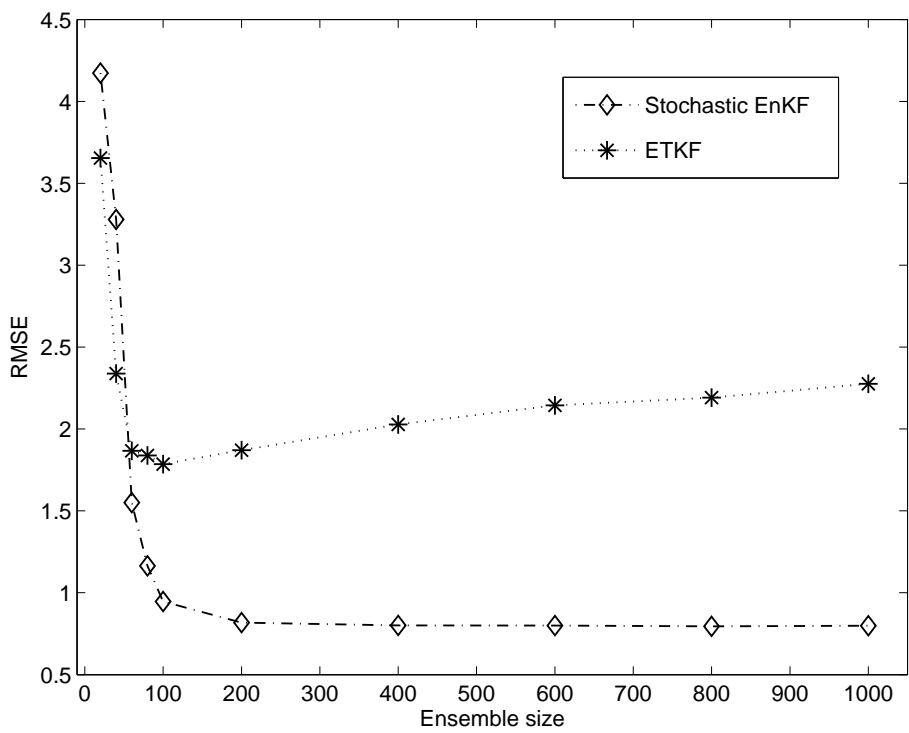
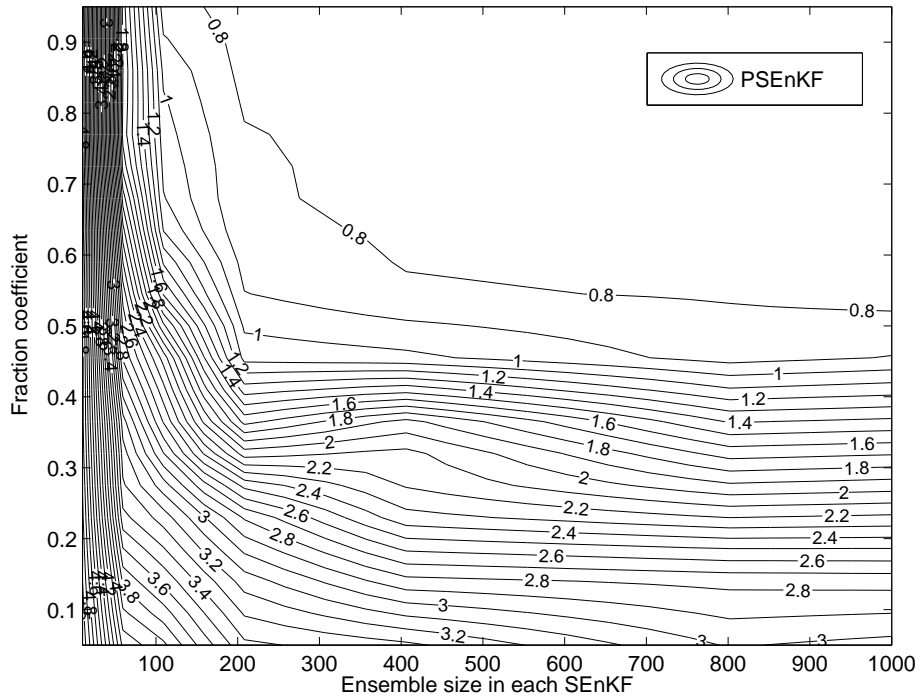


Figure 3: RMS errors (over 20 experiments) of the stochastic EnKF and the ETKF as the functions of the ensemble size.



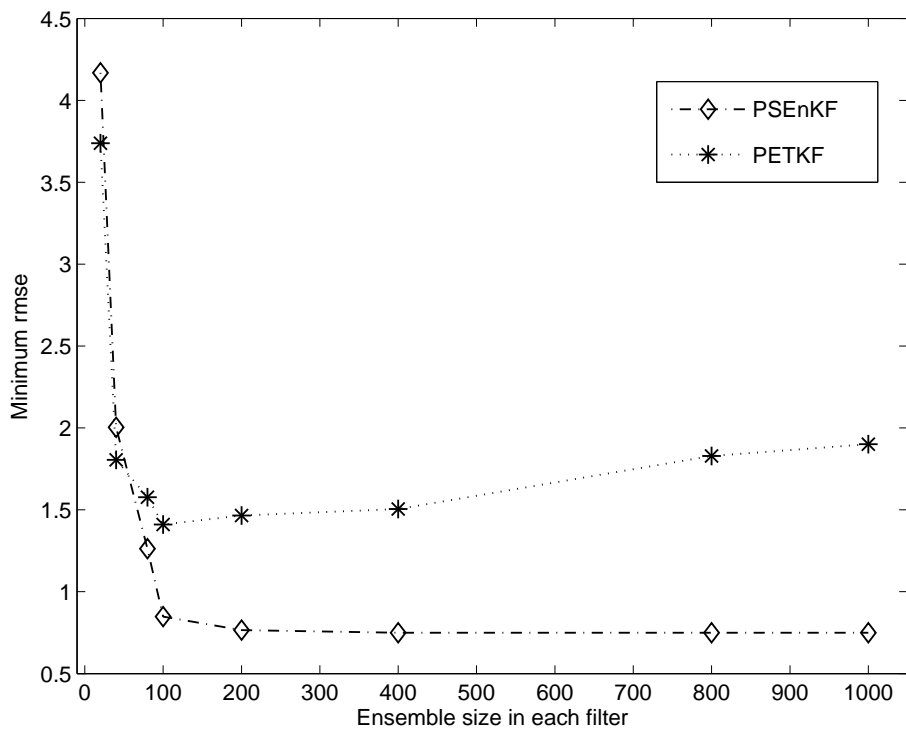
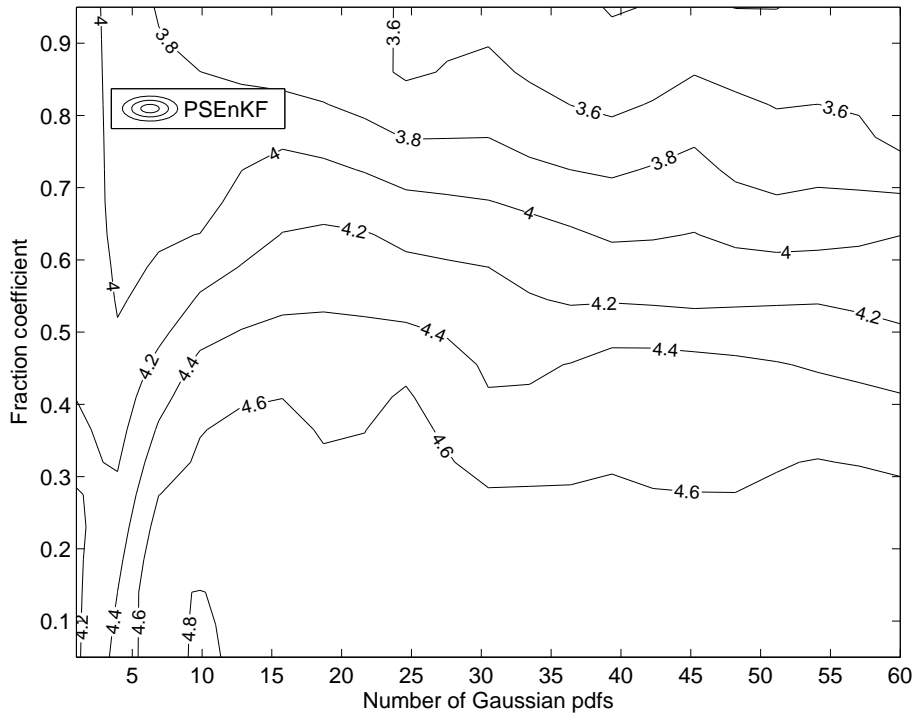
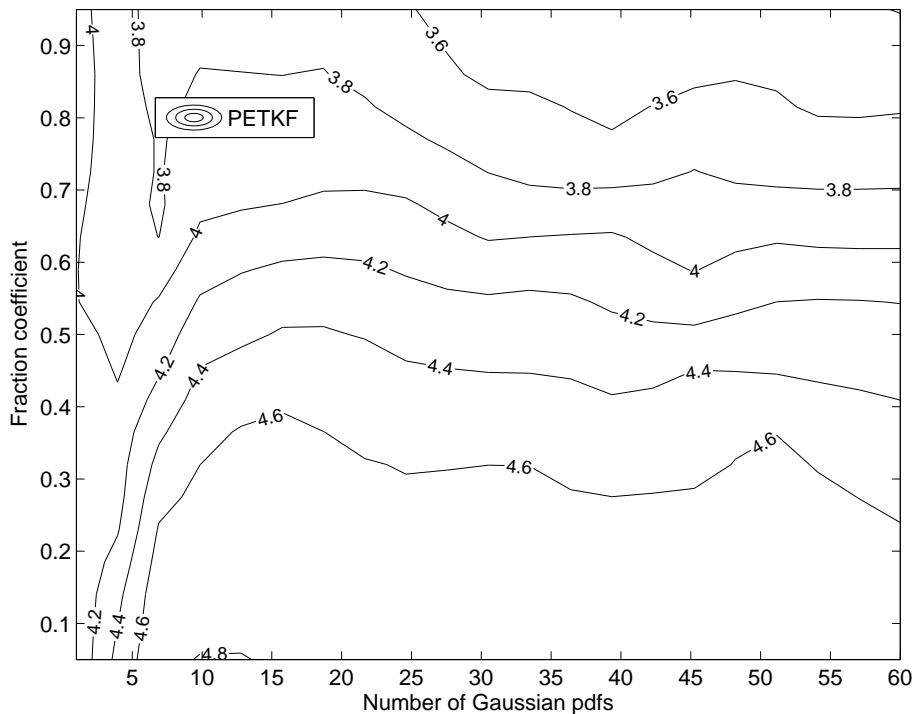


Figure 5: Minimum rms errors  $\hat{e}_{min}$  (over 20 experiments) of the stochastic EnKF and ETKF-based PEnKFs (with a fixed number of Gaussian *pdfs* of 3 in each PKF) as the function of the ensemble size in each ensemble filter.



(a) Stochastic EnKF-based PKF



(b) ETKF-based PKF

Figure 6: RMS errors (over 20 experiments) of the stochastic EnKF- and ETKF-based PEnKFs (with a fixed ensemble size of 20 in each ensemble filter) as the functions of the fraction coefficient and the number of Gaussian *pdfs* in the MON.

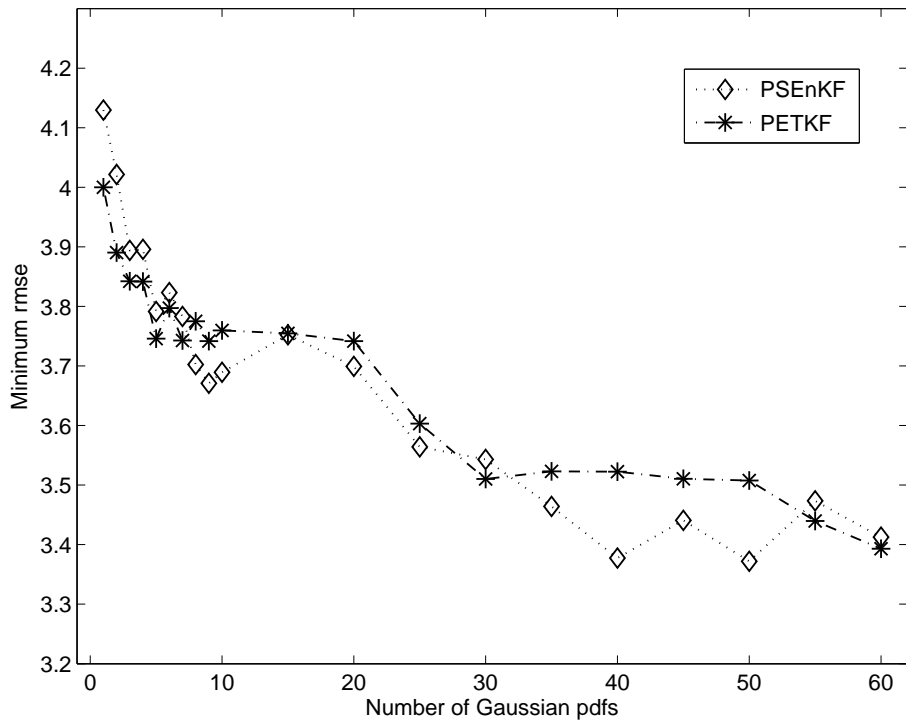


Figure 7: Minimum rms errors  $\hat{e}_{min}$  (over 20 experiments) of the stochastic EnKF- and ETKF-based PEnKFs (with a fixed ensemble size of 20 in each ensemble filter) as the function of the number of Gaussian *pdfs* in the MON.

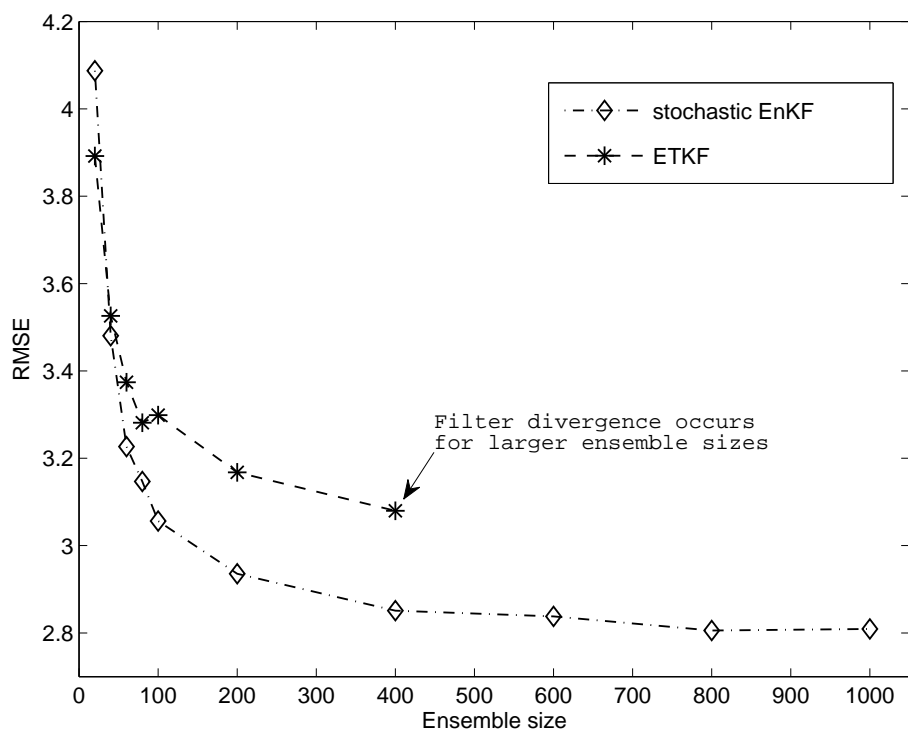
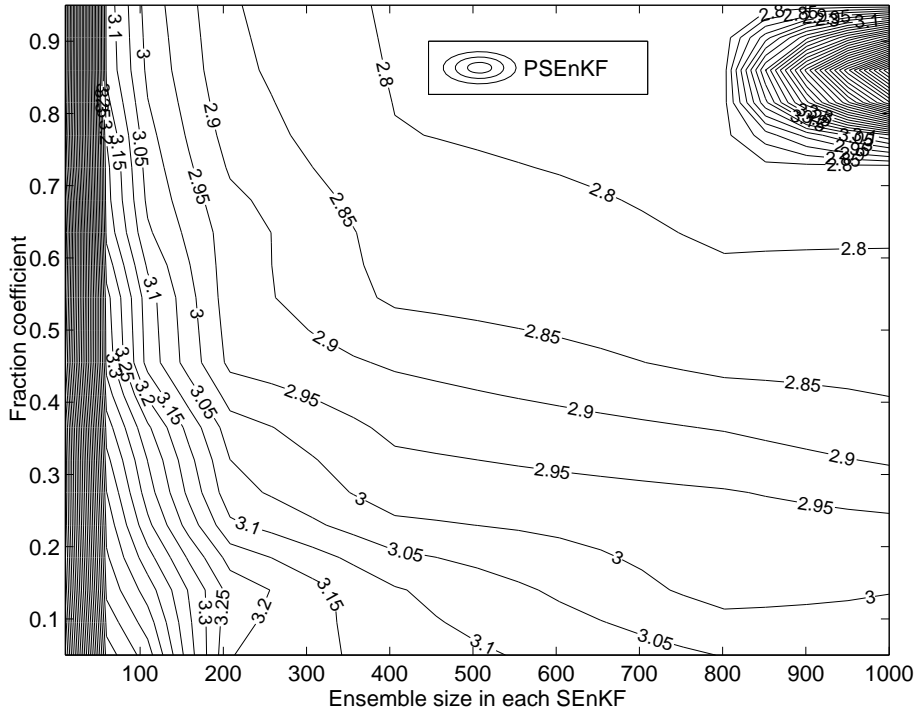
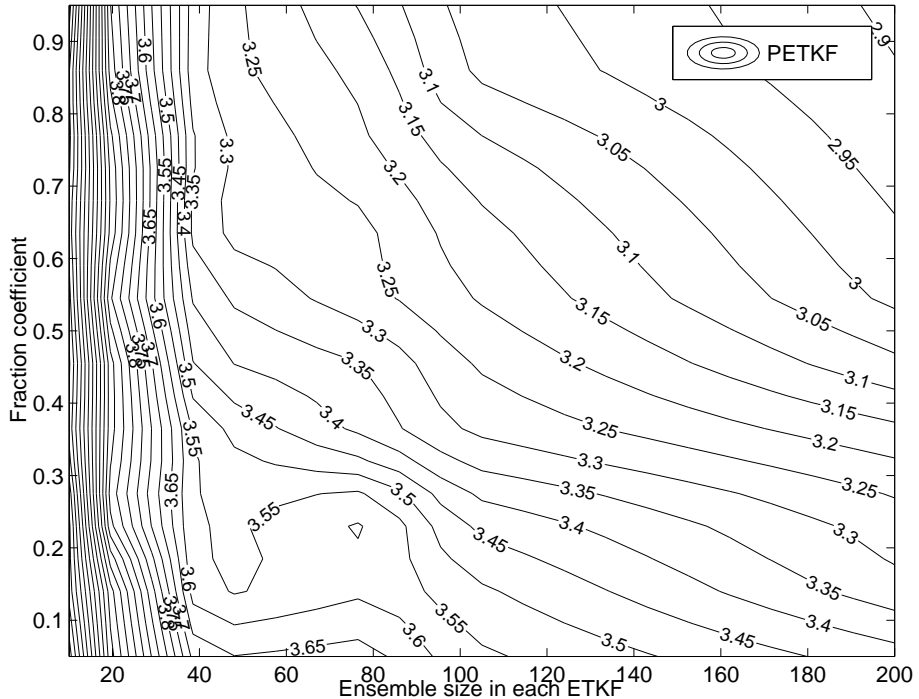


Figure 8: RMS errors (over 20 experiments) of the stochastic EnKF and the ETKF as the functions of the ensemble size.



(a) Stochastic EnKF-based PKF



(b) ETKF-based PKF

Figure 9: RMS errors (over 20 experiments) of the stochastic EnKF- and ETKF-based PEnKFs (with a fixed number of Gaussian *pdfs* of 3 in each PKF) as the functions of the fraction coefficient and the ensemble size of the ensemble filter. In Fig. 9(b) the ensemble size is reduced to 200. <sup>41</sup> Due to numerical instability

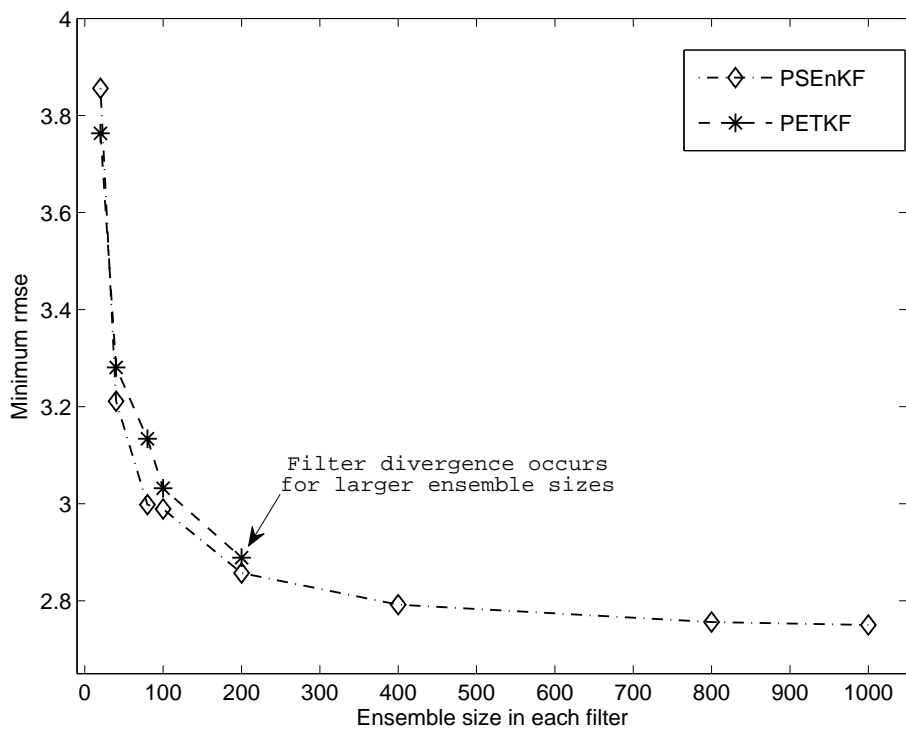


Figure 10: Minimum rms errors  $\hat{e}_{min}$  (over 20 experiments) of the stochastic EnKF- and ETKF-based PEnKFs (with a fixed number of Gaussian *pdfs* of 3 in each PKF) as the function of the ensemble size in each ensemble filter.

## 793 Support Material: The Full Re-sampling

### 794 Algorithm

795 Here we discuss how to construct the ensemble set  $\{\mathbf{X}_{en}^i, i = 1, \dots, q\}$  in the PEnKF.

796 We note that the relative positions of the dimension  $n$  of the random vector  $\mathbf{x}$ , the  
 797 number  $q$  of the Gaussian *pdfs* in the MON Eq. (13), and the ensemble size  $m$  of each  
 798 EnKF in the PKF determines our re-sampling strategies. In certain circumstances,  
 799 a singular value decomposition (SVD) may be required on the covariance matrix  $\bar{\mathbf{P}}$   
 800 in Eq. (14) such that

$$801 \bar{\mathbf{P}} = \mathbf{V} \mathbf{D} \mathbf{V}^T = \sum_{i=1}^n \sigma_i^2 \mathbf{e}_i \mathbf{e}_i^T, \quad (S.1)$$

801 where  $\mathbf{V}$  is the matrix consisting of the eigenvectors  $\mathbf{e}_i$  of  $\bar{P}$ , and  $\mathbf{D} \equiv \text{diag}(\sigma_1^2, \dots, \sigma_n^2)$   
 802 the diagonal matrix consisting of the corresponding eigenvalues  $\sigma_i^2$  (we also assume  
 803  $\sigma_i \geq 0$  without loss of generality). Depending on the values of  $q$ ,  $m$  and  $n$ , one may  
 804 avoid computing the full spectra of  $\bar{\mathbf{P}}$ , as to be shown below.

#### 805 Case I: $q \leq n$ and $m \leq n$

806 In this case the number  $q$  of (re-approximation) Gaussian distributions and the en-  
 807 semble size  $m$  are both less than the dimension  $n$  of the system state. We consider  
 808 two possibilities below.

809 1.  $q \leq m \leq n$

Here we choose

$$810 \frac{1}{q} \sum_{i=1}^q (\theta_i - \bar{\mathbf{x}}) (\theta_i - \bar{\mathbf{x}})^T = (1 - c^2) \sum_{i=1}^{q-1} \sigma_i^2 \mathbf{e}_i \mathbf{e}_i^T, \quad (S.2a)$$

$$811 \Phi = c^2 \sum_{i=1}^{q-1} \sigma_i^2 \mathbf{e}_i \mathbf{e}_i^T + \sum_{i=q}^{m-1} \sigma_i^2 \mathbf{e}_i \mathbf{e}_i^T. \quad (S.2b)$$

810 The reason to choose the superscripts  $q - 1$  and  $m - 1$  on the right hand side of  
811 Eqs. (S.2a) and (S.2b) will be made clear soon. We also note that the sum

$$\Phi + \frac{1}{q} \sum_{i=1}^q (\theta_i - \bar{\mathbf{x}}) (\theta_i - \bar{\mathbf{x}})^T = \sum_{i=1}^{n-1} \sigma_i^2 \mathbf{e}_i \mathbf{e}_i^T \quad (S.3)$$

812 is not equal to  $\bar{\mathbf{P}}$  exactly. Instead, it only adds up to the first  $(m - 1)$  terms of  $\sigma_i^2 \mathbf{e}_i \mathbf{e}_i^T$ .

813 Let  $\Theta = [\theta_1, \dots, \theta_q]$  be the collection of the means  $\theta_i$  in the MON  $\tilde{p}(\mathbf{x})$ , and

$$\mathbf{S}_\mu = \sqrt{1 - c^2} [\sigma_1 \mathbf{e}_1, \dots, \sigma_{q-1} \mathbf{e}_{q-1}]$$

814 be the square root of  $(1 - c^2) \sum_{i=1}^{q-1} \sigma_i^2 \mathbf{e}_i \mathbf{e}_i^T$  in Eq. (S.2a), then it can be verified that

$$\Theta = \bar{\mathbf{x}} \mathbf{1}_q^T + \sqrt{q} \mathbf{S}_\mu \mathbf{C}_{q-1,q} \quad (S.4)$$

815 yields a set of the means  $\theta_i$  that satisfy Eq. (S.2a), where  $\mathbf{1}_q^T$  denotes the transpose  
816 of the  $q \times 1$  column vector  $\mathbf{1}_q$  with all its elements being one (so that  $\bar{\mathbf{x}} \mathbf{1}_q^T$  consists  
817 of  $N$  identical column vectors  $\bar{\mathbf{x}}$ ), and  $\mathbf{C}_{q-1,q}$  is a  $(q - 1) \times q$  matrix satisfying that  
818  $\mathbf{C}_{q-1,q}(\mathbf{C}_{q-1,q})^T = \mathbf{I}_{q-1}$ , with  $\mathbf{I}_{q-1}$  being the  $(q - 1)$ -dimensional identity matrix,  
819 and that  $\mathbf{C}_{q-1,q} \mathbf{1}_q = \mathbf{0}_{q-1}$ , with  $\mathbf{0}_{q-1}$  being a  $(q - 1) \times 1$  column vector with all its  
820 elements being zero. The first constraint,  $\mathbf{C}_{q-1,q}(\mathbf{C}_{q-1,q})^T = \mathbf{I}_{q-1}$  guarantees that the  
821 sample covariance of  $\Theta$  satisfies the constraint in Eq. (S.2a), and the second one,  
822  $\mathbf{C}_{q-1,q} \mathbf{1}_q = \mathbf{0}_{q-1}$  guarantees that the sample mean of  $\Theta$  is equal to  $\bar{\mathbf{x}}$ , as is required  
823 in Eq. (16). For the generation of such a matrix  $\mathbf{C}_{q-1,q}$ , readers are referred to,  
824 for example, Hoteit et al. (2002); Pham (2001). In addition, since the dimension of  
825  $\mathbf{C}_{q-1,q}$  is  $(q - 1) \times q$ , we require that the dimension of the square root matrix  $\mathbf{S}_\mu$  is  
826  $n \times (q - 1)$ . Therefore, on the right hand side of Eq. (S.2a), the superscript shall be  
827  $(q - 1)$ , rather than  $q$ . The reason to use the superscript  $(m - 1)$  in Eq. (S.2b) is  
828 similar, as can be seen below.

829 To generate the ensembles  $\mathbf{X}_{en}^i$  ( $i = 1, \dots, q$ ), with  $\theta_i$  and  $\Phi$  being their sample  
830 means and covariances, we first construct the square root matrix

$$\mathbf{S}_\phi = [c\sigma_1 \mathbf{e}_1, \dots, c\sigma_{q-1} \mathbf{e}_{q-1}, \sigma_q \mathbf{e}_q, \dots, \sigma_{n-1} \mathbf{e}_{m-1}] \quad (S.5)$$

831 of  $\Phi$ , and generate  $\mathbf{X}_{en}^i$  by

$$\mathbf{X}_{en}^i = \theta_i \mathbf{1}_m^T + \sqrt{m} \mathbf{S}_\phi \mathbf{C}_{m-1,m}, \text{ for } i = 1, \dots, q, \quad (\text{S.6})$$

832 where  $\mathbf{C}_{m-1,m}$  is a matrix similar to  $\mathbf{C}_{q-1,q}$  in Eq. (S.4). We note that the term  
 833  $\sqrt{m} \mathbf{S}_\phi \mathbf{C}_{m-1,m}$  is common to all EnKFs, and thus only needs to be calculated once.  
 834 This is direct implication from the choice of the uniform covariance  $\Phi$  in  $\tilde{p}(\mathbf{x})$ , as we  
 835 have pointed out previously, which leads to computational savings in comparison to  
 836 the non-uniform choice.

837 2.  $m < q \leq n$

Here we choose

$$\frac{1}{q} \sum_{i=1}^q (\theta_i - \bar{\mathbf{x}}) (\theta_i - \bar{\mathbf{x}})^T = (1 - c^2) \sum_{i=1}^{m-1} \sigma_i^2 \mathbf{e}_i \mathbf{e}_i^T + \sum_{i=m}^{q-1} \sigma_i^2 \mathbf{e}_i \mathbf{e}_i^T, \quad (\text{S.7a})$$

$$\Phi = c^2 \sum_{i=1}^{m-1} \sigma_i^2 \mathbf{e}_i \mathbf{e}_i^T. \quad (\text{S.7b})$$

838 Now define the square root matrix

$$\mathbf{S}_\mu = [\sqrt{1 - c^2} \sigma_1 \mathbf{e}_1, \dots, \sqrt{1 - c^2} \sigma_{m-1} \mathbf{e}_{m-1}, \sigma_m \mathbf{e}_m, \dots, \sigma_{q-1} \mathbf{e}_{q-1}] \quad (\text{S.8})$$

839 of the term on right hand side of Eq. (S.7a), and the square root matrix

$$\mathbf{S}_\phi = c [\sigma_1 \mathbf{e}_1, \dots, \sigma_{n-1} \mathbf{e}_{m-1}] \quad (\text{S.9})$$

840 of  $\Phi$  in Eq. (S.7b). Then  $\theta_i$  and  $\mathbf{X}_{en}^i$  can be generated through Eqs. (S.4) and (S.6),  
 841 respectively.

842 **Case II:  $q \leq n$  and  $m > n$**

In this case the number  $q$  of Gaussian distributions is less than the dimension  $n$  of the system state, but the ensemble size  $m$  is larger than  $n$ . We choose

$$\frac{1}{q} \sum_{i=1}^q (\theta_i - \bar{\mathbf{x}}) (\theta_i - \bar{\mathbf{x}})^T = (1 - c^2) \sum_{i=1}^{q-1} \sigma_i^2 \mathbf{e}_i \mathbf{e}_i^T, \quad (\text{S.10a})$$

$$\Phi = c^2 \sum_{i=1}^{q-1} \sigma_i^2 \mathbf{e}_i \mathbf{e}_i^T + \sum_{i=q}^n \sigma_i^2 \mathbf{e}_i \mathbf{e}_i^T = \bar{\mathbf{P}} - (1 - c^2) \sum_{i=1}^{q-1} \sigma_i^2 \mathbf{e}_i \mathbf{e}_i^T. \quad (\text{S.10b})$$

843 The last equality in Eq. (S.10b) implies that one does not need to compute the full  
 844 spectra of  $\bar{\mathbf{P}}$  and the corresponding eigenvectors. Instead, one only needs to compute  
 845 the first  $(q - 1)$  terms of  $\sigma_i^2 \mathbf{e}_i \mathbf{e}_i^T$ .

846 Now define the square root matrix

$$\mathbf{S}_\mu = \sqrt{1 - c^2} [\sigma_1 \mathbf{e}_1, \dots, \sigma_{q-1} \mathbf{e}_{q-1}], \quad (\text{S.11})$$

847 so that one can again adopt Eq. (S.4) to generate  $\theta_i$  ( $i = 1, \dots, q$ ). To generate the  
 848 ensembles  $\mathbf{X}_{en}^i$ , the situation here is different from that in the previous case, in that  
 849 the ensemble size  $m$  is larger than the dimension  $n$ , so that one cannot obtain enough  
 850 ensemble members through Eq. (S.6). As a result, one may instead choose to draw  
 851  $(m - 1)$  samples  $\delta \mathbf{x}_j^\phi$  ( $j = 1, \dots, m - 1$ ) from the distribution  $N(\delta \mathbf{x} : \mathbf{0}_n, \Phi)$  to form  
 852 a matrix  $\Delta \mathbf{X}_\phi \equiv [\delta \mathbf{x}_1^\phi, \dots, \delta \mathbf{x}_{m-1}^\phi]$ . Then the ensemble  $\mathbf{X}_{en}^i$  is produced via

$$\mathbf{X}_{en}^i = \theta_i \mathbf{1}_m^T + \Delta \mathbf{X}_\phi \mathbf{C}_{m-1,m}, \quad \text{for } i = 1, \dots, q. \quad (\text{S.12})$$

853 Eq. (S.12) is similar to the partial re-sampling scheme in Hoteit et al. (2008), although  
 854 here the perturbation term  $\Delta \mathbf{X}_\phi \mathbf{C}_{m-1,m}$  can be common to all EnKFs, and thus can  
 855 be drawn only once to reduce computational cost.

856 **Case III:  $q > n$  and  $m \leq n$**

In this case the ensemble size  $m$  is no larger than the dimension  $n$  of the system state, but the number  $q$  of Gaussian distributions is. We choose

$$\frac{1}{q} \sum_{i=1}^q (\theta_i - \bar{\mathbf{x}}) (\theta_i - \bar{\mathbf{x}})^T = (1 - c^2) \sum_{i=1}^{m-1} \sigma_i^2 \mathbf{e}_i \mathbf{e}_i^T + \sum_{i=m}^n \sigma_i^2 \mathbf{e}_i \mathbf{e}_i^T = \bar{\mathbf{P}} - c^2 \sum_{i=1}^{m-1} \sigma_i^2 \mathbf{e}_i \mathbf{e}_i^T, \quad (\text{S.13a})$$

$$\Phi = c^2 \sum_{i=1}^{m-1} \sigma_i^2 \mathbf{e}_i \mathbf{e}_i^T. \quad (\text{S.13b})$$

857 Since  $q > n$ , we choose to draw  $(q - 1)$  samples  $\delta \mathbf{x}_j^\mu$  from the distribution  $N(\delta \mathbf{x} : 858 \mathbf{0}_n, \bar{\mathbf{P}} - c^2 \sum_{i=1}^{m-1} \sigma_i^2 \mathbf{e}_i \mathbf{e}_i^T)$  to form a matrix  $\Delta \mathbf{X}_\mu \equiv [\delta \mathbf{x}_1^\mu, \dots, \delta \mathbf{x}_{q-1}^\mu]$ , while  $\theta_i$  are generated by

$$\Theta = \bar{\mathbf{x}} \mathbf{1}_q^T + \Delta \mathbf{X}_\mu \mathbf{C}_{q-1,q}. \quad (\text{S.14})$$

860 Let

$$\mathbf{S}_\phi = c[\sigma_1 \mathbf{e}_1, \dots, \sigma_{n-1} \mathbf{e}_{m-1}], \quad (\text{S.15})$$

861 then  $\mathbf{X}_{en}^i$  can be generated through Eq. (S.6).

862 **Case IV:  $q > n$  and  $m > n$**

863 In this case both the number  $q$  of Gaussian distributions and the ensemble size  $m$  864 are larger than the dimension  $n$  of the system state. We let  $\Phi = c^2 \bar{\mathbf{P}}$  and define 865  $\mathbf{P}_n = (1 - c^2) \bar{\mathbf{P}}$ . To generate  $\theta_i$ , we first draw  $(q - 1)$  samples  $\delta \mathbf{x}_j^\mu$  from the distribution 866  $N(\delta \mathbf{x} : \mathbf{0}_n, \mathbf{P}_n)$  to form a matrix  $\Delta \mathbf{X}_\mu = [\delta \mathbf{x}_1^\mu, \dots, \delta \mathbf{x}_{q-1}^\mu]$ , and then apply Eq. (S.14). 867 Meanwhile, we also draw  $(m - 1)$  samples  $\delta \mathbf{x}_j^\phi$  from the distribution  $N(\delta \mathbf{x} : \mathbf{0}_n, \Phi)$  to 868 form a matrix  $\Delta \mathbf{X}_\phi \equiv [\delta \mathbf{x}_1^\phi, \dots, \delta \mathbf{x}_{m-1}^\phi]$ , and then apply Eq. (S.12) to generate the 869 ensembles  $\mathbf{X}_{en}^i$ .

